RM L50A23a

NACA

RESEARCH MEMORANDUM

LOW-SPEED PRESSURE-DISTRIBUTION MEASUREMENTS AT A REYNOLDS NUMBER OF 3.5 × 10^6 ON A WING WITH LEADING-EDGE SWEEPBACK DECREASING FROM 45° AT THE ROOT TO 20° AT THE TIP

By U. Reed Barnett, Jr. and Roy H. Lange

Langley Aeronautical Laboratory
Langley Air Force Base, Va.

NATIONAL ADVISORY COMMITTEE FOR AERONAUTICS

WASHINGTON
July 7, 1950

NACA RM L50A23a

NATIONAL ADVISORY COMMITTEE FOR AERONAUTICS

RESEARCH MEMORANDUM

LOW-SPEED PRESSURE-DISTRIBUTION MEASUREMENTS AT A REYNOLDS NUMBER OF 3.5×10^6 ON A WING WITH LEADING-EDGE SWEEPBACK DECREASING FROM 45° AT THE ROOT TO 20° AT THE TIP

By U. Reed Barnett, Jr. and Roy H. Lange

SUMMARY

Results are presented of an investigation to determine the pressure distributions on a wing with leading-edge sweepback decreasing from 45° at the root to 20° at the tip, an aspect ratio of 4.12, taper ratio of 0.36, and NACA 64A009 airfoil sections. Tests were conducted at a Reynolds number of 3.5×10^6 and a Mach number of 0.07 on the wing with and without 0.20 chord 0.65 span split flaps deflected 60°. These pressure distributions are analysed herein to determine the character of flow and its effect on the stability of the wing.

INTRODUCTION

Some consideration has been given to a sweptback wing with the sweep decreasing from root to tip as a means of alleviating the poor low-speed characteristics of sweptback wings. The selection of this particular plan form is based on the premise that the smaller angle of sweepback in the outboard wing panels would diminish the inherent early tip-stalling tendencies and thus improve the low-speed stability and control characteristics. Tests at low scale of this type of sweptback wing (reference 1) show, for low-speed conditions, increments in lift due to plain flap deflection which are considerably higher than those measured for conventional sweptback wings and a linear variation of pitching-moment coefficient with lift coefficient up to the stall. In view of the favorable results at low scale, a general investigation of a sweptback wing with the leading-edge sweep decreasing from 45° at the root to 20° at the tip has been conducted in the Langley full-scale tunnel. The maximum lift and static-longitudinal stability characteristics

of the wing for a Reynolds number range from 2.4×10^6 to 6.0×10^6 are discussed in reference 2. The present paper presents the results of pressure-distribution measurements made on the wing to determine the chordwise and spanwise loadings and to aid in the evaluation of the flow over a wing plan form of this type.

The investigation consisted in measurements of the surface static pressures along the chord for stations located at 10, 20, 40, 60, and 80 percent of the wing semispan at angles of attack from 0° through the stall at zero yaw. The basic wing and the wing with 60° split flaps installed were tested at a Reynolds number of about 3.5×10^6 and a Mach number of 0.07.

COEFFICIENTS AND SYMBOLS

The data are referred to the wing axes with the origin at the quarter-chord of the mean aerodynamic chord. The data have been reduced to standard NACA nondimensional coefficients which are defined as follows:

C_L lift coefficient $\left(\frac{\text{Lift}}{qS}\right)$

C_L' lift coefficient $\left(\int_0^1 c_l \frac{c}{c_{av}} d\frac{2y}{b}\right)$

C_m pitching-moment coefficient $\left(\frac{\text{Pitching moment}}{qSc}\right)$

C_m' pitching-moment coefficient $\left(\frac{c_{av}}{\bar{c}} \int_0^1 c_n \frac{\bar{x}}{c}\left(\frac{c}{c_{av}}\right)^2 d\frac{2y}{b}\right)$

$\bar{x}$ distance from local center of pressure to quarter-chord of the mean aerodynamic chord

c_n section normal-force coefficient $\left(\int_0^1 P_r \, d\frac{x}{c}\right)$

c_l approximate section lift coefficient $\left(\cos\alpha \int_0^1 P_r \, d\frac{x}{c} \text{ or } c_n \cos\alpha\right)$

P_r $P_{lower} - P_{upper}$

P	pressure coefficient $\left(\frac{p - p_o}{q}\right)$
p	local static pressure
p_o	free-stream static pressure
q	free-stream dynamic pressure
$\frac{c_l c}{C_L c_{av}}$	span loading coefficient
c	local chord
c_{av}	average chord $\left(\frac{S}{b}\right)$
$\bar{c}$	mean aerodynamic chord $\left(\frac{2}{S}\int_0^{b/2} c^2 dy\right)$
S	wing area
b	wing span
y	spanwise coordinate, perpendicular to plane of symmetry
x	chordwise coordinate, parallel to plane of symmetry
α	angle of attack, degrees
δ_f	split-flap deflection, degrees

MODEL AND TESTS

The geometric characteristics of the model are given in figure 1. The wing has an angle of sweepback at the leading edge of 45° for the inboard 30 percent span, 30° for the midsemispan (35 percent) and 20° for the outboard 35 percent span. The wing has NACA 64A009 airfoil sections parallel to the plane of symmetry, an aspect ratio of 4.12, taper ratio of 0.36, and has no geometric dihedral or twist. A more detailed description of the model construction is given in reference 2.

The wing was equipped with flush surface static pressure orifices arranged in chordwise rows located at 10, 20, 40, 60, and 80 percent

of the right wing semispan as shown in figure 2. The chordwise location of the orifices, which is the same for all spanwise stations, is also given in figure 2. A photograph of the basic wing mounted in the Langley full-scale tunnel is given as figure 3.

The wing was equipped with a 20-percent-chord split flap deflected 60° located on the inboard 65 percent of the wing span. The flap was equipped with one static pressure orifice for each spanwise station at the midpoint of the flap chord which, when projected vertically to the airfoil chord, was located at 85 percent of the local airfoil chord.

The surface static pressures were measured by means of a multiple-tube manometer and photographically recorded. Tests were made at zero yaw through an angle-of-attack range from 0° through the stall, taken in increments of 4° except near maximum lift where 1° increments were used. The configurations tested were the basic wing and the wing with a 20-percent-chord inboard 65-percent-span split flap deflected 60°. All tests were made at a Reynolds number of 3.5×10^6 and a Mach number of 0.07. Studies of flow characteristics were also made for these configurations by the use of wool tufts attached to the wing upper surface.

REDUCTION OF DATA

Pressure Distributions

The measured static pressures were reduced to coefficient form and plotted against their respective chordwise locations. For the wing with the split flap deflected, the flap static pressures were plotted perpendicular to the airfoil chord. For these figures a uniform pressure field was assumed to exist behind the flap, the value being determined by the orifice located at 0.95c on the lower surface of the airfoil. Because of the insufficient data to determine accurately the span loadings at the end of the flap and the wing tips, the curves were faired in these regions according to the best available information.

From these pressure plots the section lift coefficients, span loading coefficients, and local centers of pressure were obtained by the usual calculation and integration procedures, neglecting the chord forces. Calculations indicate a maximum error due to neglecting chord forces of about 2 percent on the wing lift coefficient and about 3 percent on the section lift coefficients.

The data have been corrected for air-stream inclination, the blocking effects, and for the jet-boundary effects. The latter correction was determined for a wing of the same span with an elliptic loading, but having an unswept plan form.

Flow Diagrams

The flow diagrams represent the combined interpretation of tuft studies and pressure distributions. In the high-lift range it was difficult to distinguish between stalled and very rough flow as indicated by the tufts and, for this reason, the pressure distributions were used to identify more precisely the stalled areas. The tufts were also used to indicate direction of flow and the degree of roughness.

RESULTS AND DISCUSSION

Presentation of Results

In figure 4 are presented the chordwise pressure distributions at several angles of attack for the basic wing, and the distributions for the wing with the split flap are shown in figure 5. The flow diagrams are presented in figure 6. In figures 7 to 9 are presented the integrated results of the pressure distributions in the form of section lift coefficients and span loading coefficients. The center-of-pressure locations are given in figures 10 and 11. The variation of the total wing lift and pitching-moment coefficients with angle of attack is given in figure 12. It should be noted that the wing lift coefficients given in figure 12 are about 5 percent and 9 percent higher, respectively, for the split flap and basic wing configuration than for the corresponding values obtained from the force measurements (reference 2). There is no explanation for these descrepancies; however, it is felt that these results do not significantly alter the conclusions derived from the data presented herein.

Pressure Distributions and Flow Characteristics

Basic wing.- The general shape of the chordwise pressure distributions at the low and moderate angles of attack are typical of the two-dimensional distributions for similar airfoils, and the flow is smooth below an angle of attack of 10°. A small region of constant pressure, indicating a local region of separated flow, first appeared near the upper-surface leading edge at an angle of attack of about 3.5°. This phenomenon is shown more clearly at the inboard panel at an angle of attack of 7.2° (fig. 4(c)). Previous two-dimensional investigations of similar airfoils (references 3 and 4) also reveal the existence of this separation bubble. Because of the small size of the bubble, investigation of this region with tufts failed to detect any disturbance.

The high leading-edge peak pressures near the angle of attack for the maximum section lift coefficient for each section are characteristic of thin airfoils. The slight hump in the pressure distributions near 0.40c was also noted in the two-dimensional tests of similar airfoil sections.

The stall was characterized by leading-edge separation, which appeared first at the outboard panel at an angle of attack of 12.8° (fig. 4(f)) and progressed inboard to the midsemispan panel as the angle of attack was increased to 14.7° (fig. 6(a)). At an angle of attack of 12.8° the flow diagrams show spanwise flow beginning at the midsemispan panel trailing edge, and with a small increase in angle of attack, reversed or forward flow appeared near the junction with the outboard panel, with the flow curving inboard along the leading edge. This appeared as a circulatory flow pattern, centered on the midsemispan wing panel and rotating in a clockwise direction on the left wing. This peculiar flow pattern appeared before complete stall had developed at the 80-percent station. The effect of this unusual type flow is to cause a considerable reduction in the leading-edge peak negative pressure as shown for the 60-percent station at an angle of attack of 13.8° (fig. 4(g)). Some separation of flow at the trailing edge is also indicated, but there is no indication from the pressures of flow breakdown at the leading edge. These results indicate that the observed unsteady reversed flow (fig. 6(a)) is confined to an attached turbulent boundary layer and does not, in this case, appear to indicate stall. The observed in-flow at the midsemispan panel leading edge is induced by the higher negative pressure peaks farther inboard. As the angle of attack was further increased, this circulating flow extended both inboard and outboard until at 18.7° it covered about 70 percent of the wing semispan.

Split flap installed.- The pressure distributions for the wing with the split flap installed (fig. 5) show higher negative pressure peaks and earlier separation than were encountered with the basic wing. Leading-edge separation first appeared at the outboard panel at an angle of attack of 9.3° (fig. 5(e)), and at the midsemispan panel of an angle of attack of 10.2° (fig. 5(f)). At the highest angle tested, 13.1°, the outboard panel was almost completely separated with the midsemispan panel being intermittently stalled behind the separated region at the leading edge.

The circulating flow pattern is also present for this configuration (fig. 6(b)), and is very similar in appearance and progression to that exhibited by the basic wing.

Section Lift Coefficient

Basic wing.— The section lift curves (fig. 7) show that the midsemispan panel maintains a higher section lift coefficient below the stall than the rest of the wing. The 60-percent station, although in the same wing panel as the 40-percent stations, reaches maximum lift about 3° earlier. This earlier stall and consequent lower $c_{l_{max}}$ is attributed to the reversed boundary-layer flow at this station discussed in the section on flow characteristics. Although the angle of attack was increased to 18.7° the section lift curves show that the 10- and 20-percent stations, which were located on the more highly swept inboard panel, had not reached maximum lift. The slight discrepancies in section lift coefficients observed at zero angle of attack are believed to be caused by possible variation in the air stream across the test section and inaccuracies in model construction.

Split flap installed.— The addition of the split flap caused a large increase in section lift coefficient (fig. 7(b)), particularly at the midsemispan panel. The 40-percent station experienced an increase in lift coefficient at zero angle of attack of 0.72, which was the highest measured on the wing for this condition. The greatest increment in maximum section lift coefficient due to flaps was 0.50, also obtained at the 40-percent station.

Span Load Distribution

Basic wing.— The span load distributions (fig. 8) are approximately elliptical in shape in the low and moderate lift range. Above an angle of attack of 10.9°, there is a steady increase and inboard shift in peak load coefficient caused by the inboard progression of stall. When the unusual circulatory type flow first appeared at an angle of attack of 13.8° it did not cause any violent change in the span load distribution.

For comparative purposes a calculated additional span load distribution, obtained by the charts of reference 5, is included in figure 8. The angle of sweepback used for these charts was 30°, which is the angle of sweepback of the midsemispan panel, with the aspect ratio and taper ratio unchanged. Although it is recognized that there is considerable difference between the assumed plan form and actual plan form, there is good agreement between the experimental and calculated additional loading curves for moderate angles of attack.

Split flap installed.— The effect of the split flap on the span loading curve is to provide an increase in loading over the flapped portion of the wing, this effect being more pronounced for low angles of attack (fig. 9). This effect is also indicated by the inboard location of center of pressure noted for the flapped wing (fig. 10). The center

of pressure moves outboard with increasing angle of attack up to 9.3° where the outboard panel reaches $c_{l_{max}}$. As angle of attack is further increased there is an inboard shift in center of pressure caused by the increase in lift of the inboard panel, which continues through the highest angle of attack tested.

Center of Pressure

Basic wing.– The chordwise center–of–pressure variation with angle of attack is presented in figure 11(a). Below the stall the local center of pressure remains essentially constant with angle of attack above an angle of attack of about 4°, but with the onset of leading–edge separation there is an abrupt rearward shift in center of pressure and a subsequent relocation at a position farther aft. Even though there is an inboard shift in wing center of pressure after the occurrence of leading–edge separation, the rearward shift in the local center of pressure combined with the maintained maximum lift of the tip sections results in satisfactory static longitudinal stability of the wing through stall, as shown in figure 12 and discussed in the force–test results of reference 2.

Split flap installed.– The effects of split–flap deflection (fig. 11(b)) is to cause a small but consistent forward movement of local center of pressure with an increase in angle of attack at all stations below the stall. The forward movement in center of pressure at the low and moderate angles of attack results in a pronounced destabilizing tendency in the wing pitching–moment characteristics for angles of attack between 6.5° and 8.3° as shown in reference 2. As leading–edge separation develops the curves follow the same trends as shown for the basic wing, with the center of pressure considerably farther aft than for the basic wing.

SUMMARY OF RESULTS

The results of an investigation at high Reynolds numbers and low Mach numbers in the Langley full–scale tunnel to determine the pressure distributions of a wing with the leading–edge sweepback decreasing from 45° at the root to 20° at the tips are summarized as follows:

1. The stall was characterized by leading–edge separation, which first occurred at the outboard panel at an angle of attack of 12.8° for the basic wing. An increase in angle of attack to 14.7° extended this separation to the midsemispan panel with the inboard panel remaining

smooth at 18.7°. For the flapped wing the stall progression was the same with leading-edge separation occurring about 3.5° earlier.

2. The 40-percent station maintains the highest section lift coefficient for all angles of attack below the stall, both with split flaps removed and installed. The greatest increment in section lift coefficient gained by use of the split flap at zero angle of attack was 0.72 measured at the 40-percent station.

3. The spanwise load distributions are approximately elliptical in shape in the moderate-lift range. The peak load coefficient is located at the inboard panel in the high-lift range. The effect of the split flap was to increase considerably the loading coefficient over the flapped portion of the wing, particularly in the low-lift range.

4. In the low-lift range the center of pressure shows little variation with angle of attack for the basic wing, but an abrupt rearward shift occurs with leading-edge separation, which, in the absence of any appreciable spanwise center-of-pressure movement, results in satisfactory static longitudinal stability. The center-of-pressure pattern is the same for the flapped wing, except for a small forward movement with increasing angle of attack below the stall. The center of pressure is located farther aft than on the basic wing.

Langley Aeronautical Laboratory
National Advisory Committee for Aeronautics
Langley Air Force Base, Va.

REFERENCES

1. Krüger, W.: Six-Component Measurements on a Cranked Swept-Back Wing. Reps. and Translations No. 816, British M.A.P. Völkenrode, Jan. 15, 1947.

2. Lange, Roy H.: Maximum-Lift Characteristics of a Wing with the Leading-Edge Sweepback Decreasing from 45° at the Root to 20° at the Tip at Reynolds Numbers from 2.4×10^6 to 6.0×10^6. NACA RM L50A04a, 1950.

3. Gault, Donald E.: Boundary-Layer and Stalling Characteristics of the NACA 63-009 Airfoil Section. NACA TN 1894, 1949.

4. McCullough, George B., and Gault, Donald E.: Boundary-Layer and Stalling Characteristics of the NACA 64A006 Airfoil Section. NACA TN 1923, 1949.

5. DeYoung, John: Theoretical Additional Span Loading Characteristics of Wings with Arbitrary Sweep, Aspect Ratio, and Taper Ratio. NACA TN 1491, 1947.

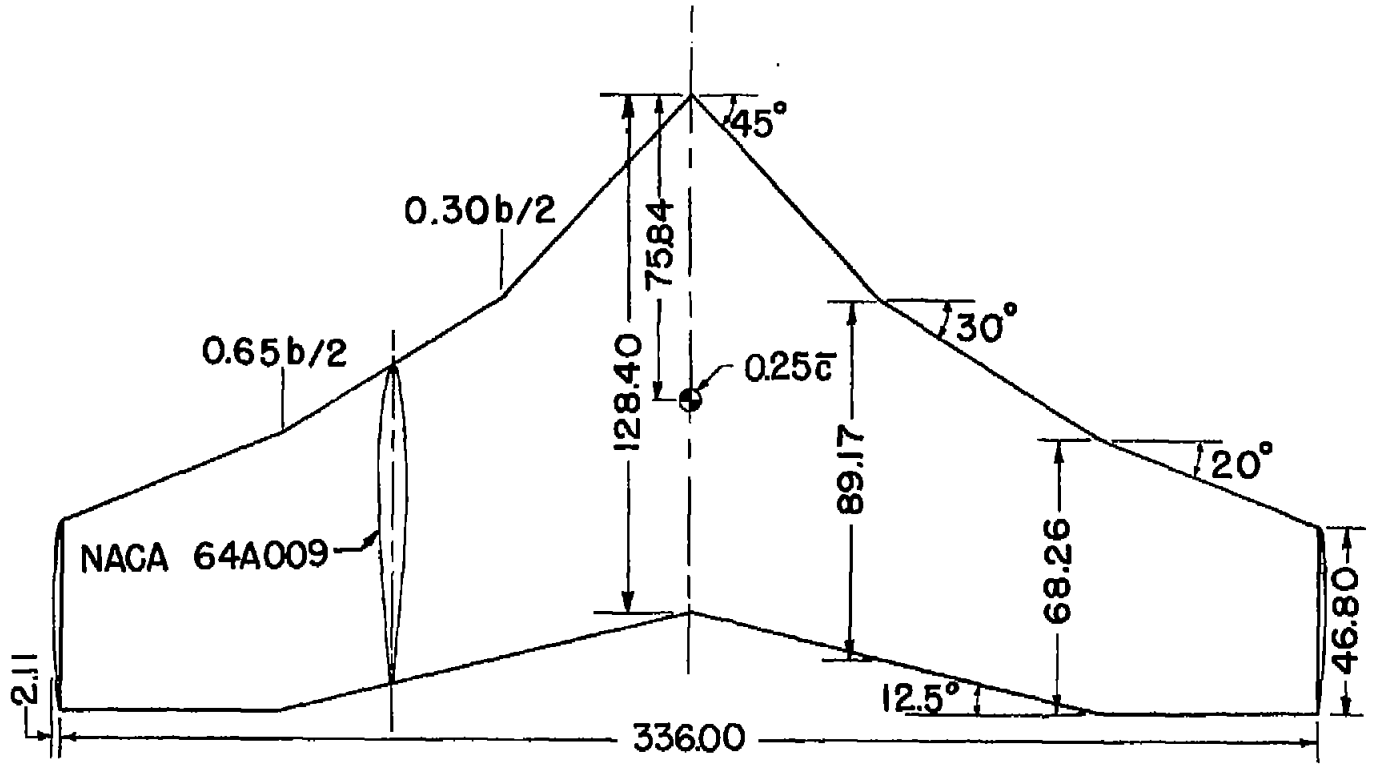

Aspect ratio	4.12	
Taper ratio	0.36	
Wing area	190.24	sq ft

Figure 1.- Geometric characteristics of wing. All dimensions are given in inches.

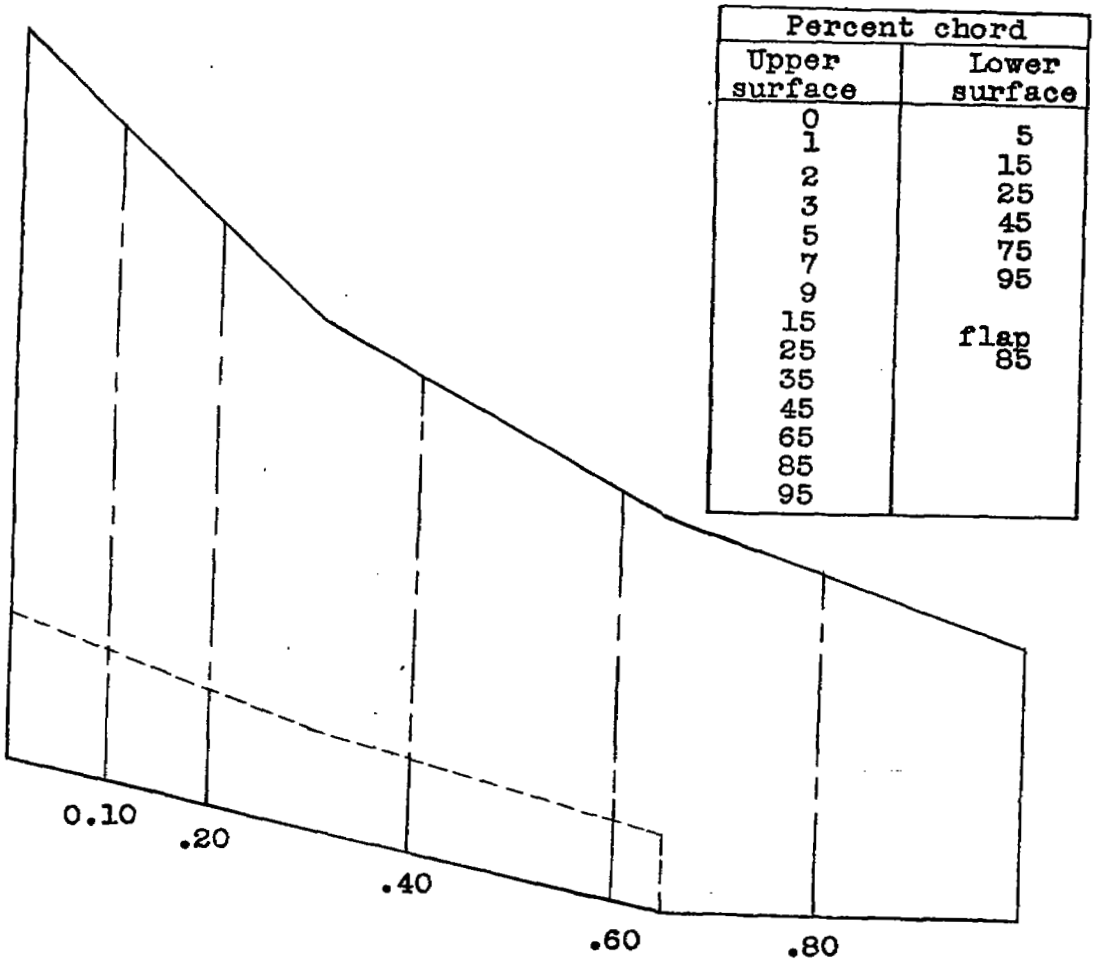

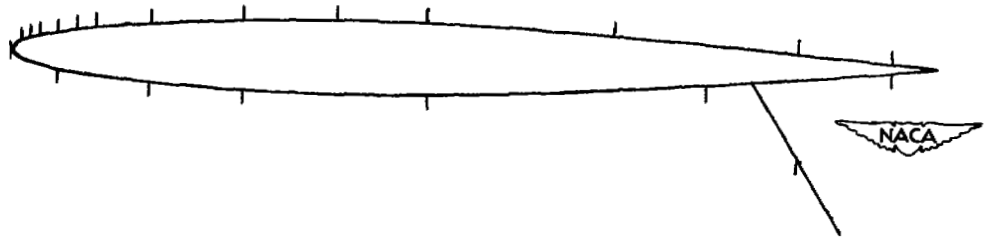

Figure 2.- Location of pressure orifices.

smooth at 18.7°. For the flapped wing the stall progression was the same with leading-edge separation occurring about 3.5° earlier.

2. The 40-percent station maintains the highest section lift coefficient for all angles of attack below the stall, both with split flaps removed and installed. The greatest increment in section lift coefficient gained by use of the split flap at zero angle of attack was 0.72 measured at the 40-percent station.

3. The spanwise load distributions are approximately elliptical in shape in the moderate-lift range. The peak load coefficient is located at the inboard panel in the high-lift range. The effect of the split flap was to increase considerably the loading coefficient over the flapped portion of the wing, particularly in the low-lift range.

4. In the low-lift range the center of pressure shows little variation with angle of attack for the basic wing, but an abrupt rearward shift occurs with leading-edge separation, which, in the absence of any appreciable spanwise center-of-pressure movement, results in satisfactory static longitudinal stability. The center-of-pressure pattern is the same for the flapped wing, except for a small forward movement with increasing angle of attack below the stall. The center of pressure is located farther aft than on the basic wing.

Langley Aeronautical Laboratory
National Advisory Committee for Aeronautics
Langley Air Force Base, Va.

REFERENCES

1. Krüger, W.: Six-Component Measurements on a Cranked Swept-Back Wing. Reps. and Translations No. 816, British M.A.P. Völkenrode, Jan. 15, 1947.

2. Lange, Roy H.: Maximum-Lift Characteristics of a Wing with the Leading-Edge Sweepback Decreasing from 45° at the Root to 20° at the Tip at Reynolds Numbers from 2.4×10^6 to 6.0×10^6. NACA RM L50A04a, 1950.

3. Gault, Donald E.: Boundary-Layer and Stalling Characteristics of the NACA 63-009 Airfoil Section. NACA TN 1894, 1949.

4. McCullough, George B., and Gault, Donald E.: Boundary-Layer and Stalling Characteristics of the NACA 64A006 Airfoil Section. NACA TN 1923, 1949.

5. DeYoung, John: Theoretical Additional Span Loading Characteristics of Wings with Arbitrary Sweep, Aspect Ratio, and Taper Ratio. NACA TN 1491, 1947.

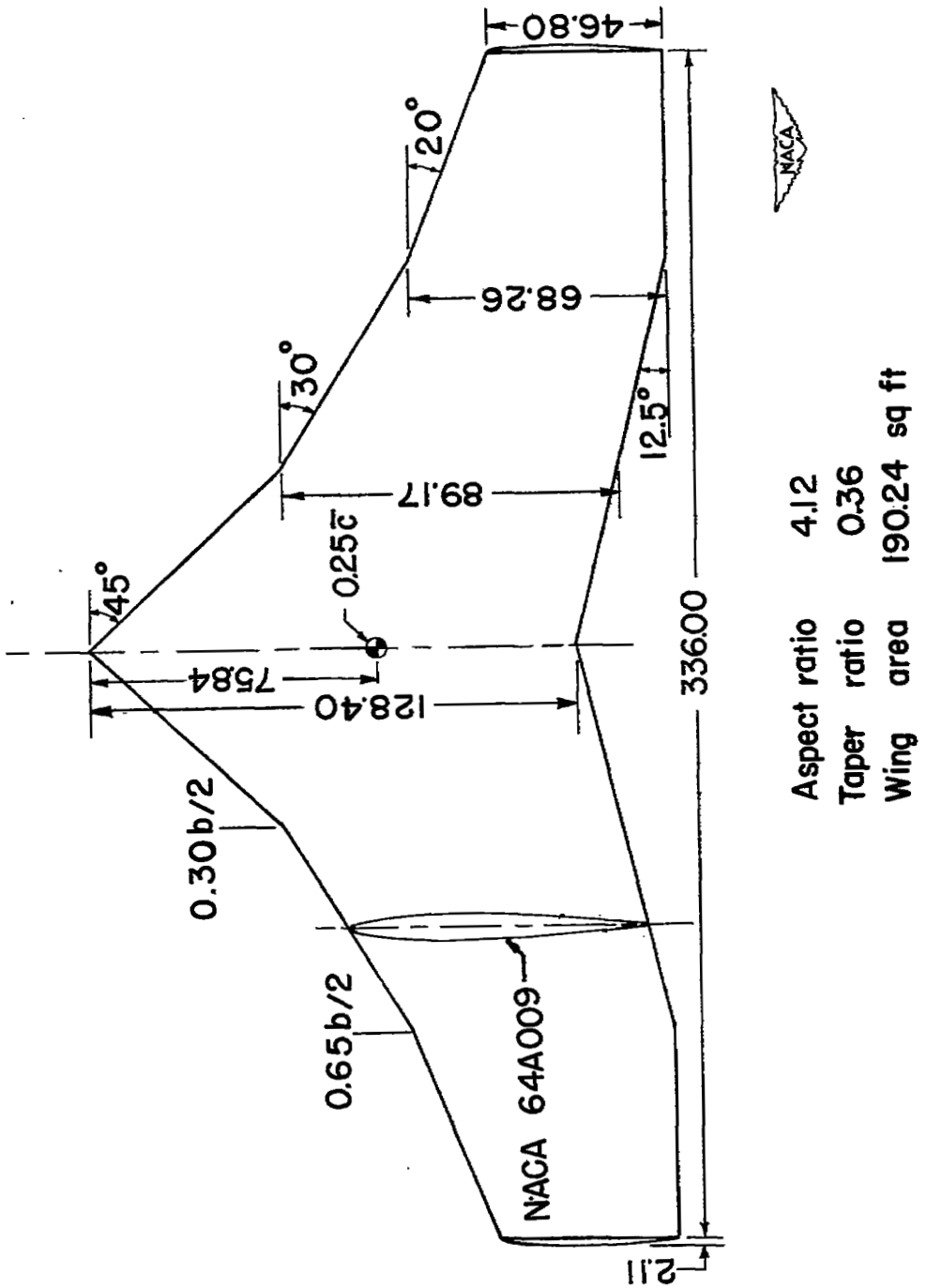

Figure 1.- Geometric characteristics of wing. All dimensions are given in inches.

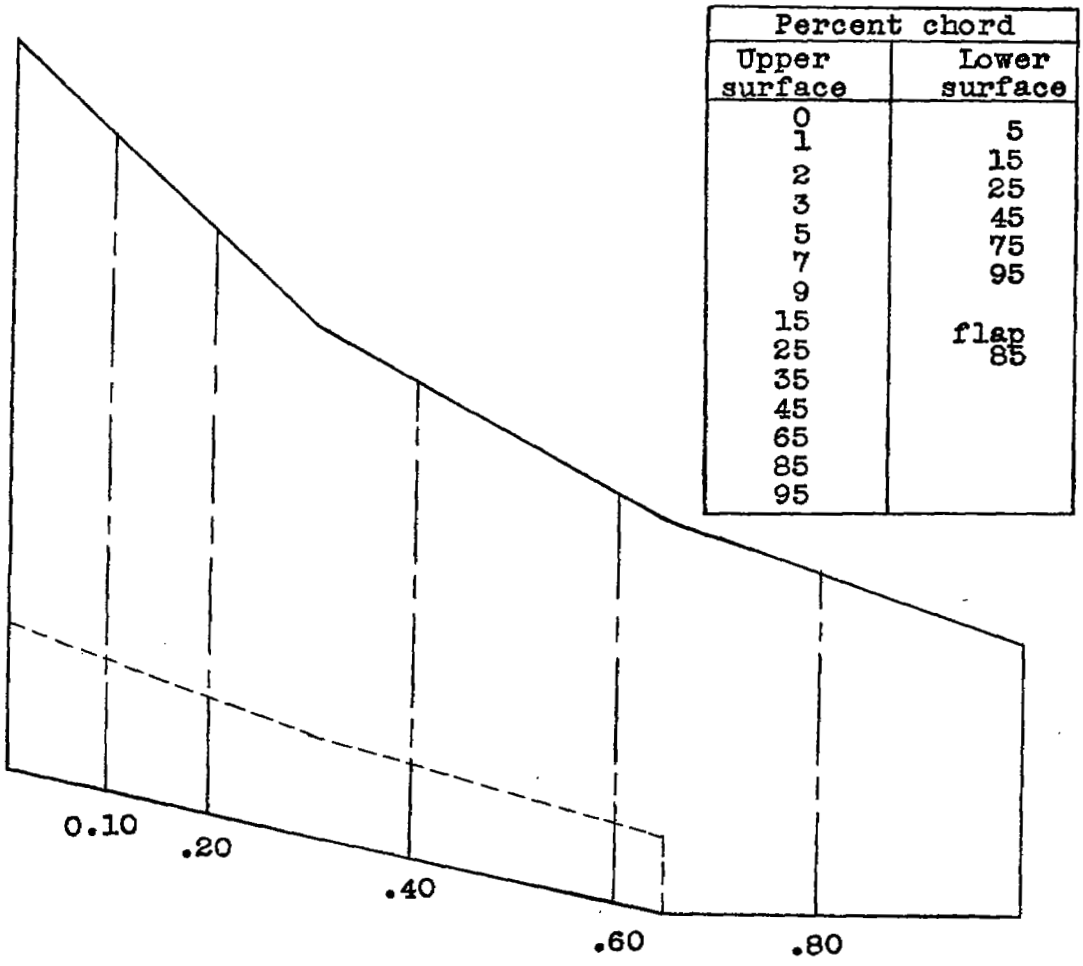

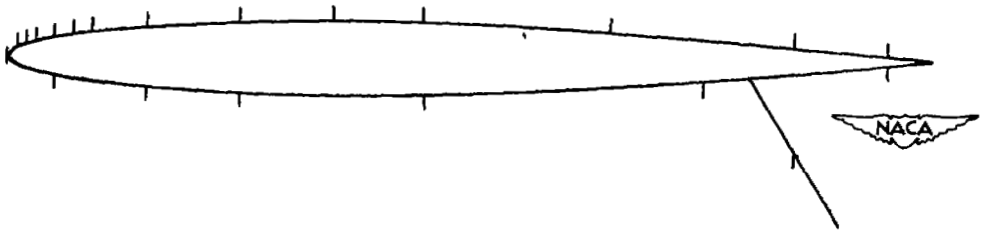

Figure 2.- Location of pressure orifices.

Figure 3.- Photograph of basic wing mounted in the Langley full-scale tunnel.

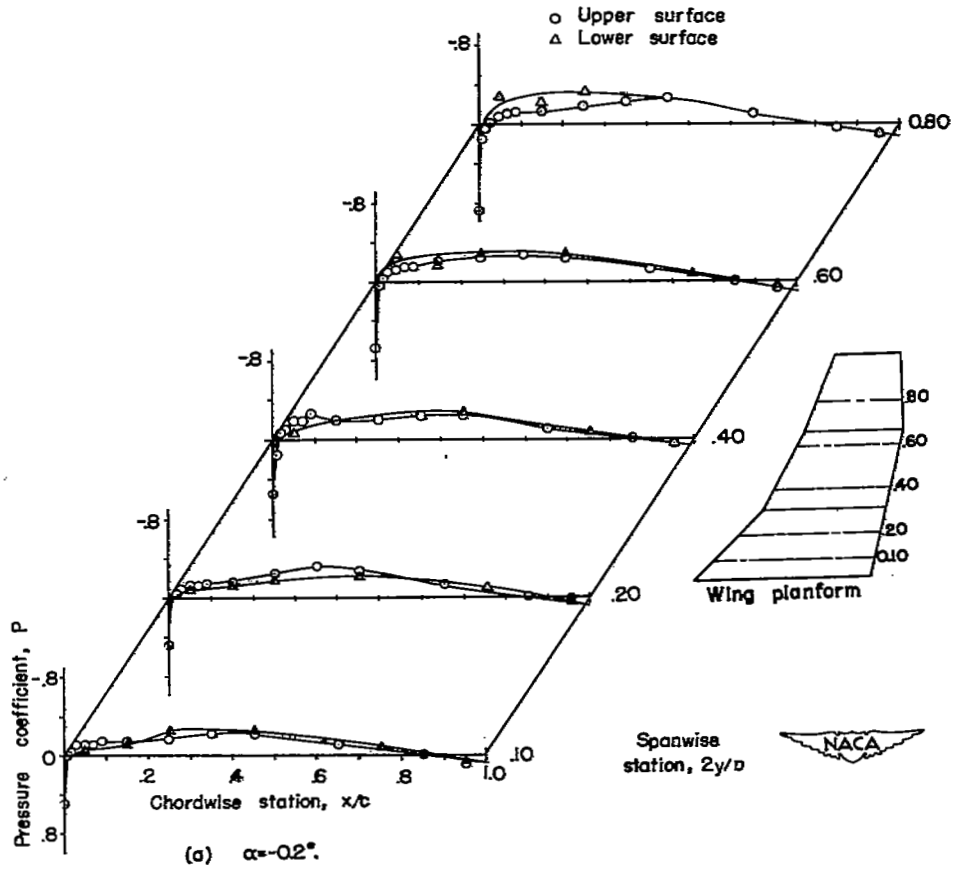

Figure 4.- Pressure distribution along the chord for five spanwise stations at various angles of attack. Basic wing.

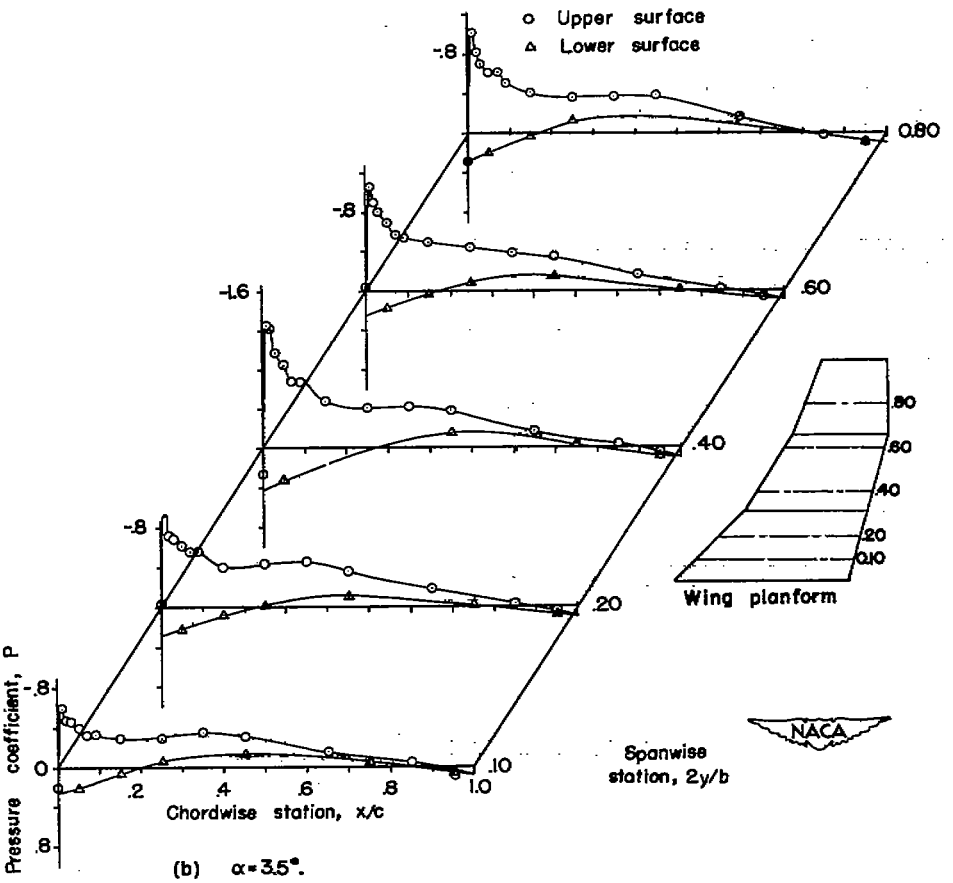

Figure 4.- Continued.

Figure 3.- Photograph of basic wing mounted in the Langley full-scale tunnel.

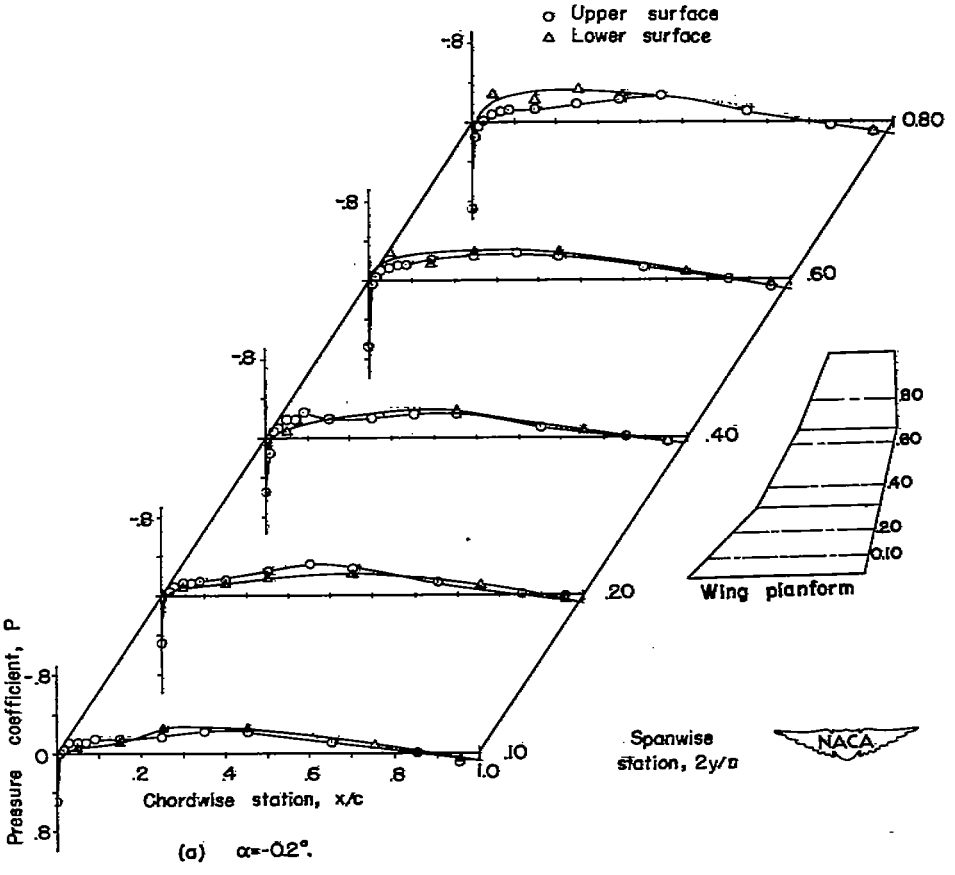

Figure 4.- Pressure distribution along the chord for five spanwise stations at various angles of attack. Basic wing.

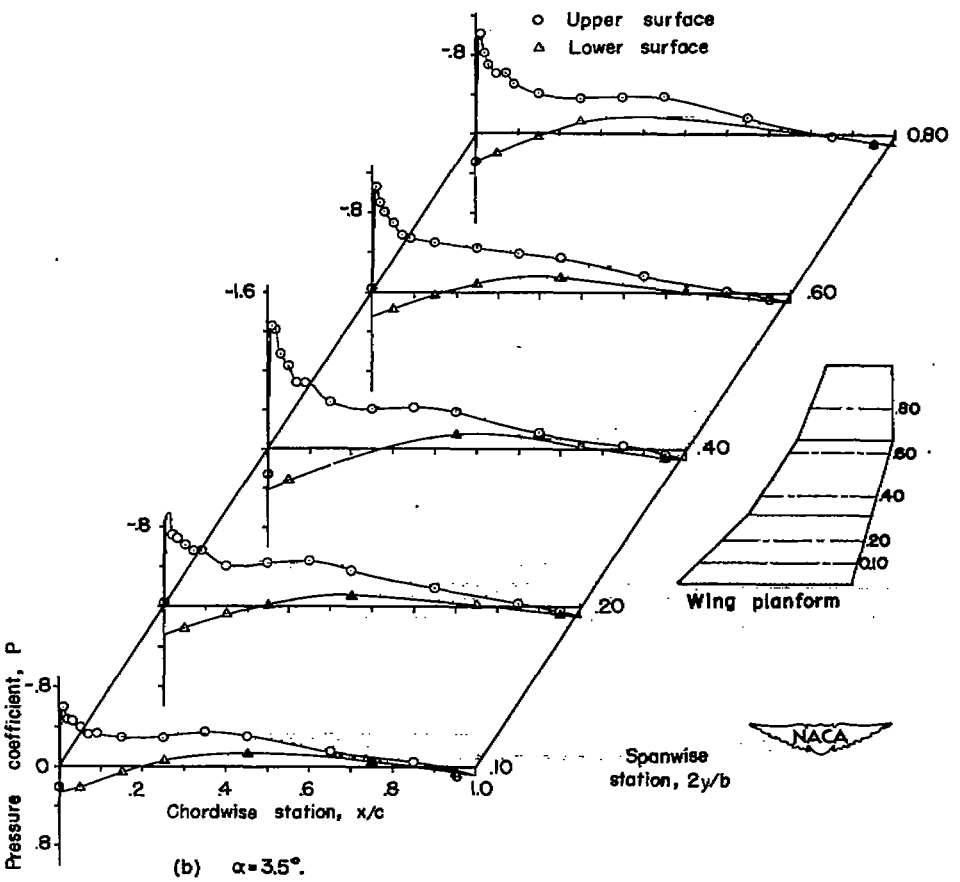

Figure 4.- Continued.

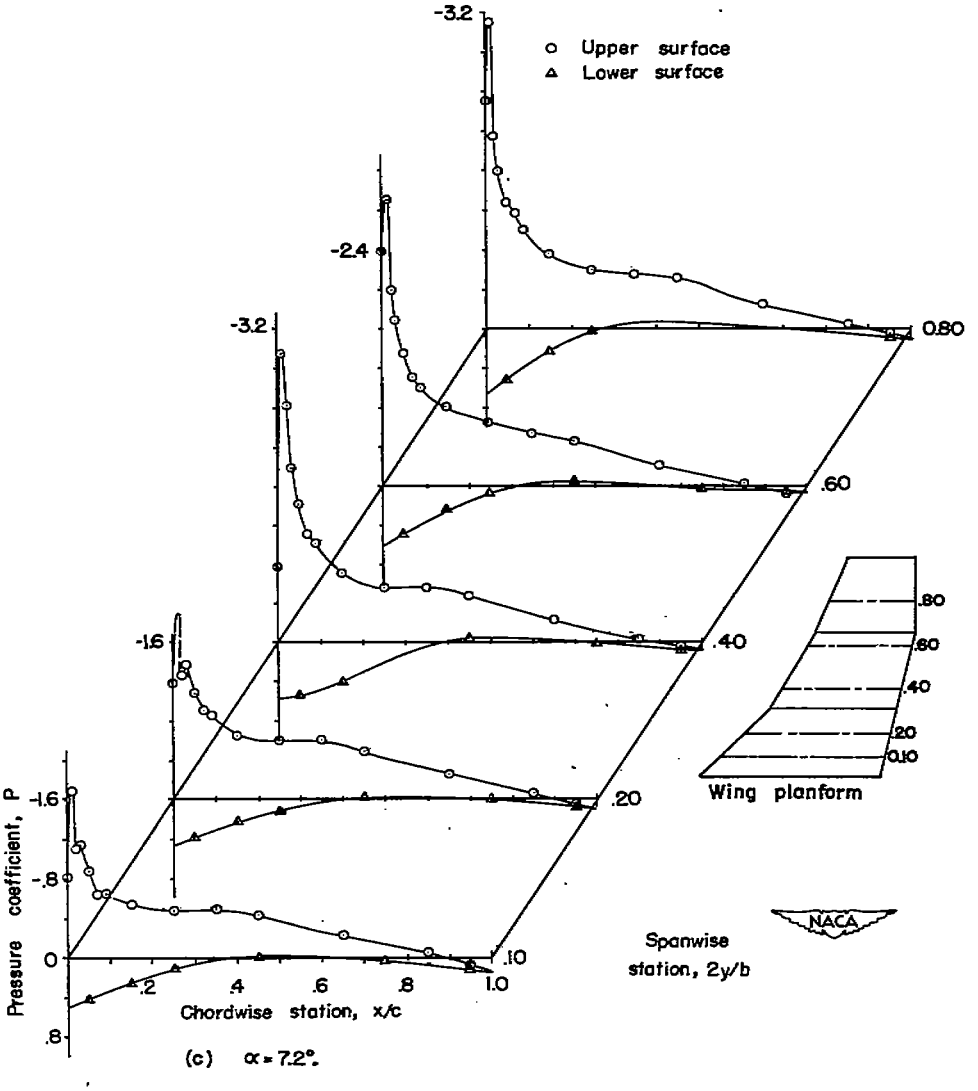

Figure 4.- Continued.

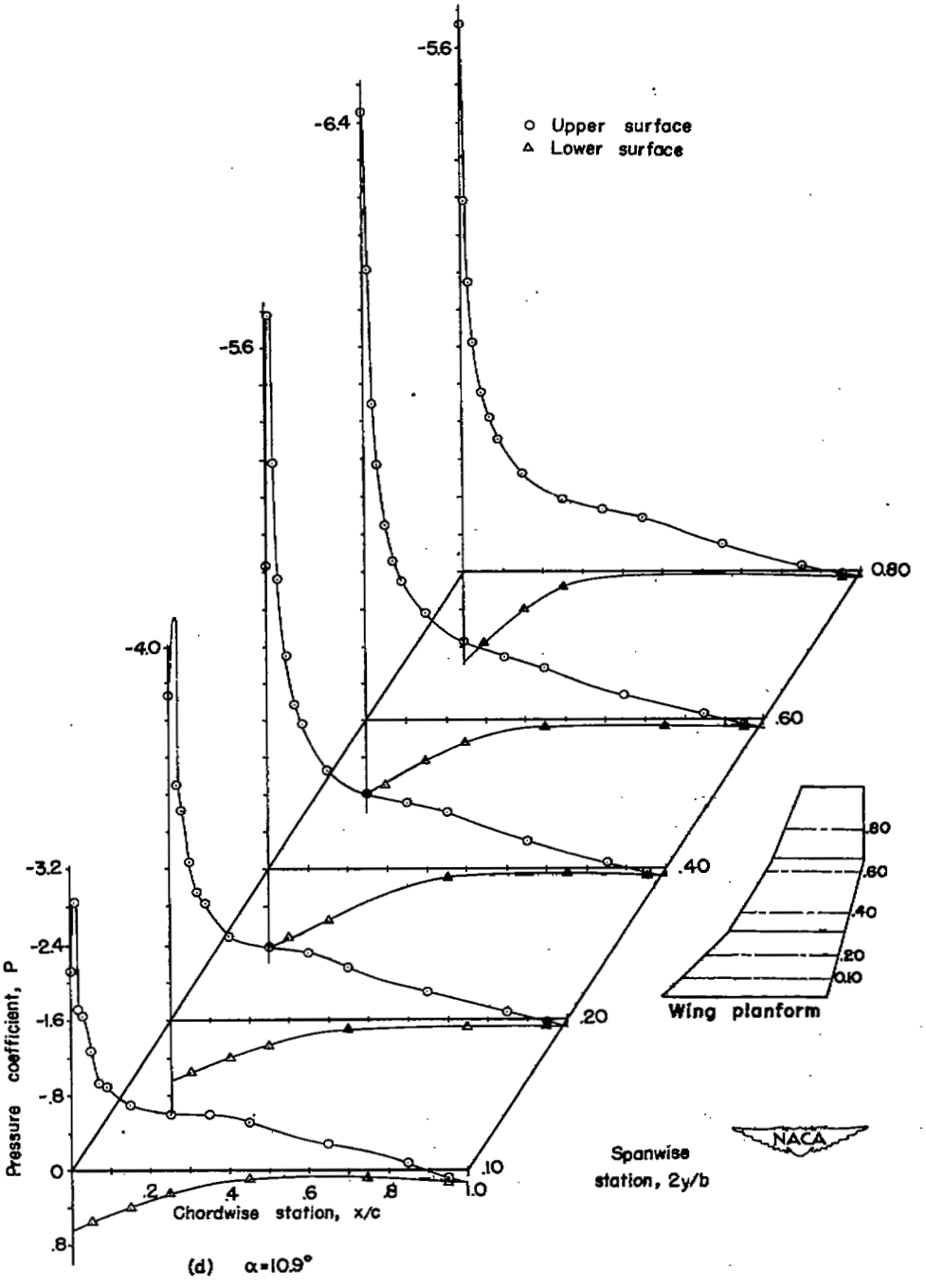

Figure 4.- Continued.

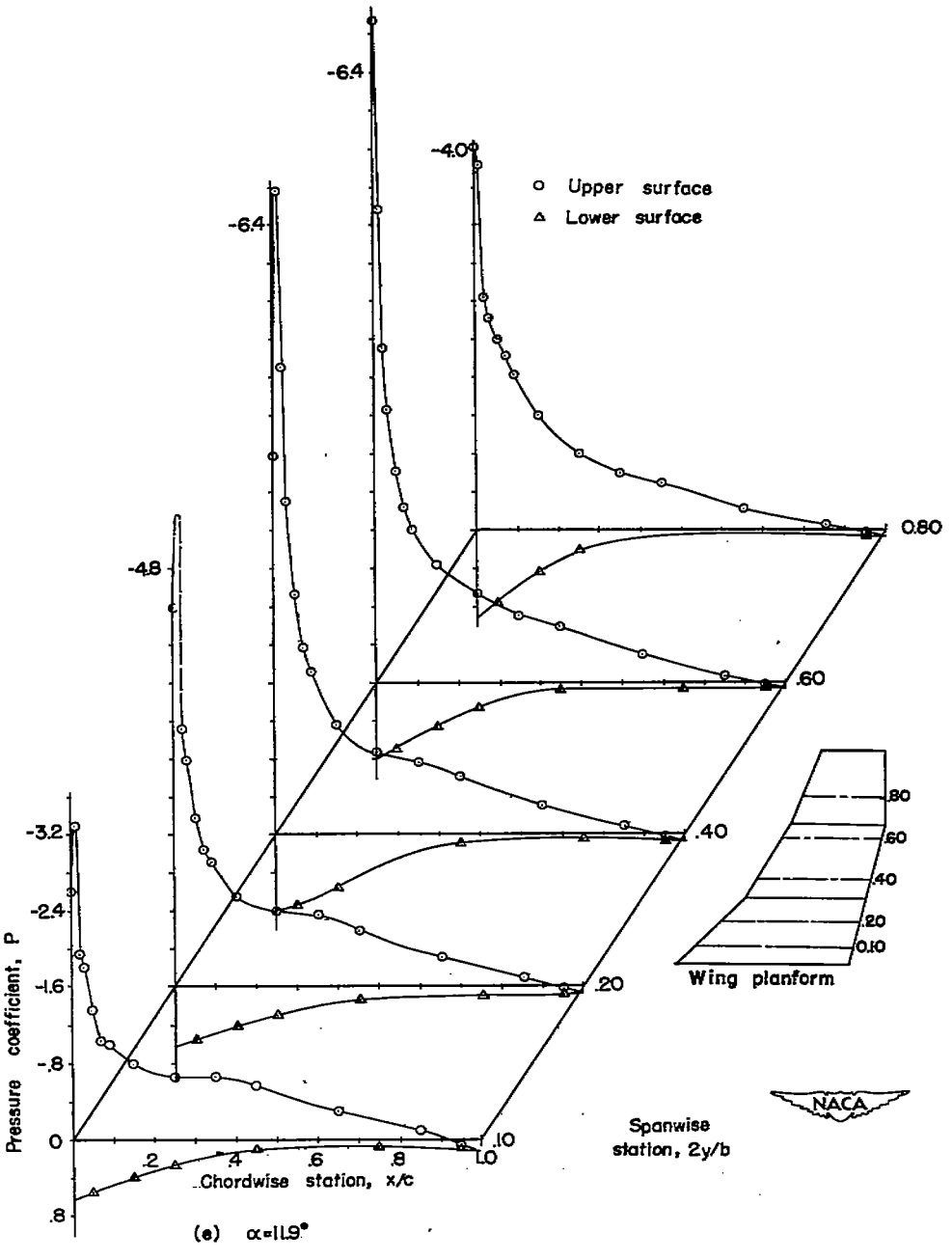

Figure 4.- Continued.

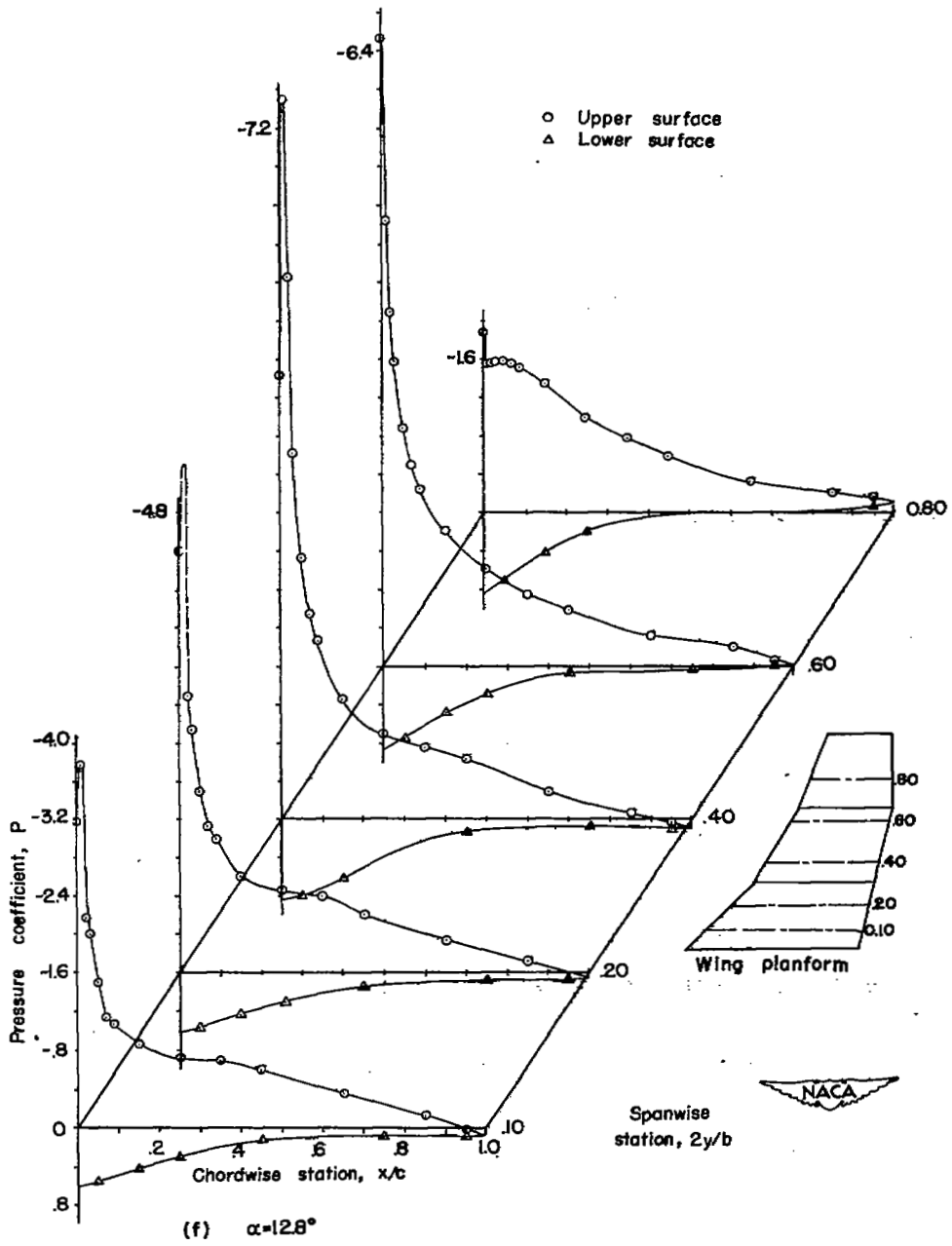

Figure 4.- Continued.

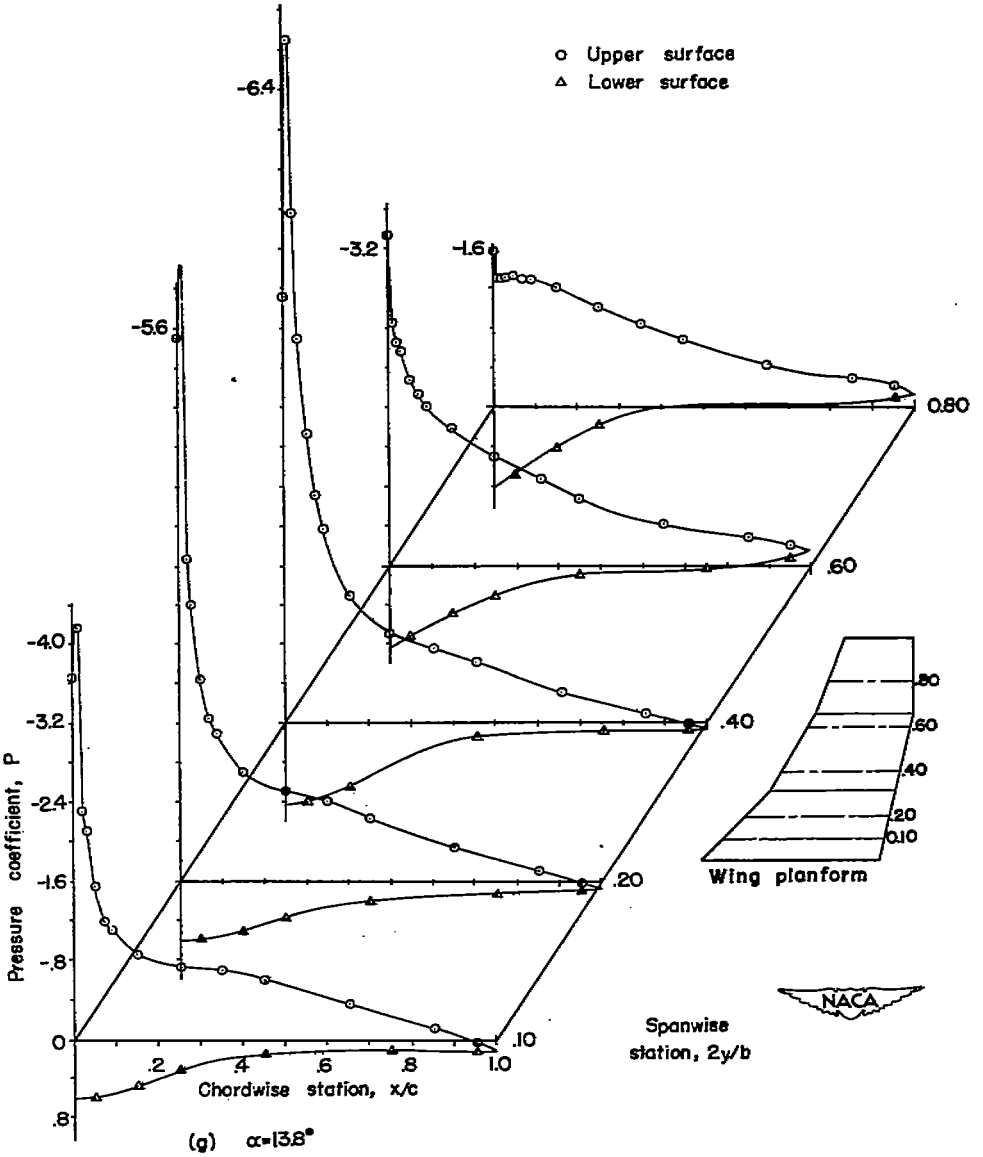

Figure 4.- Continued.

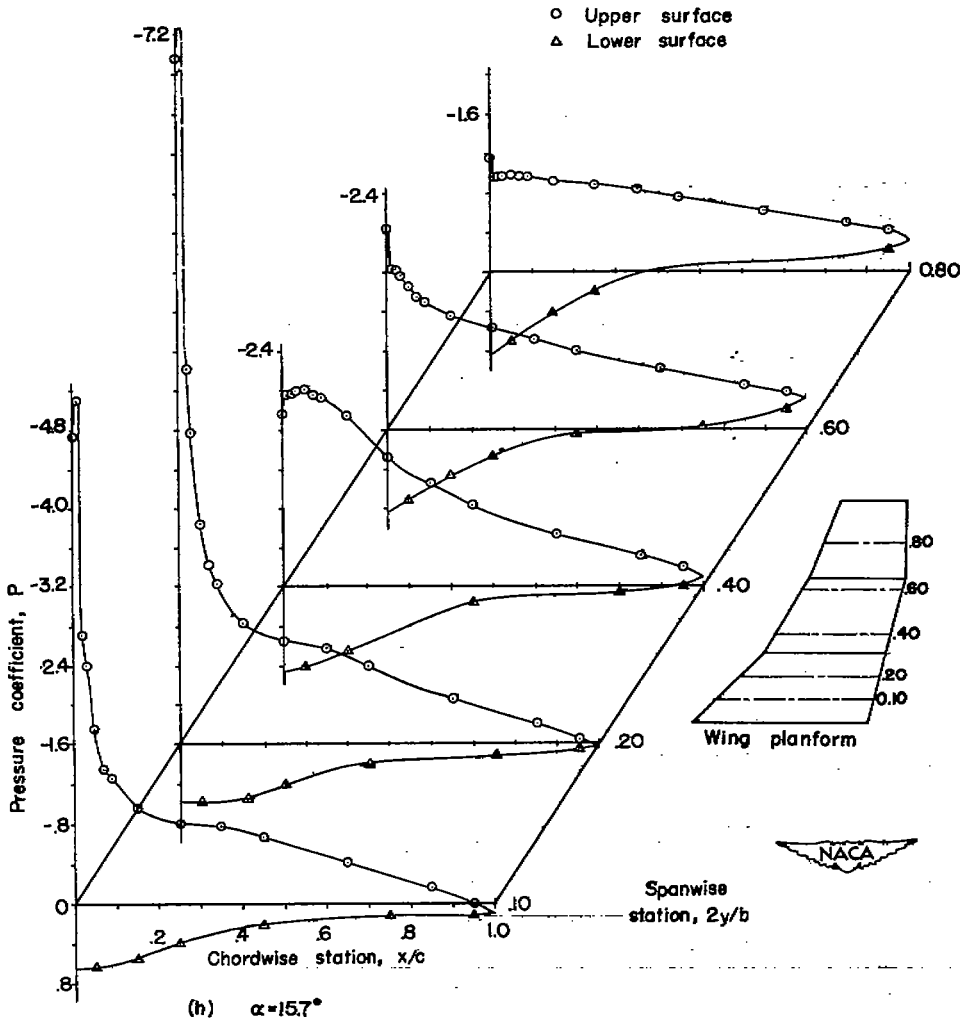

Figure 4.- Continued.

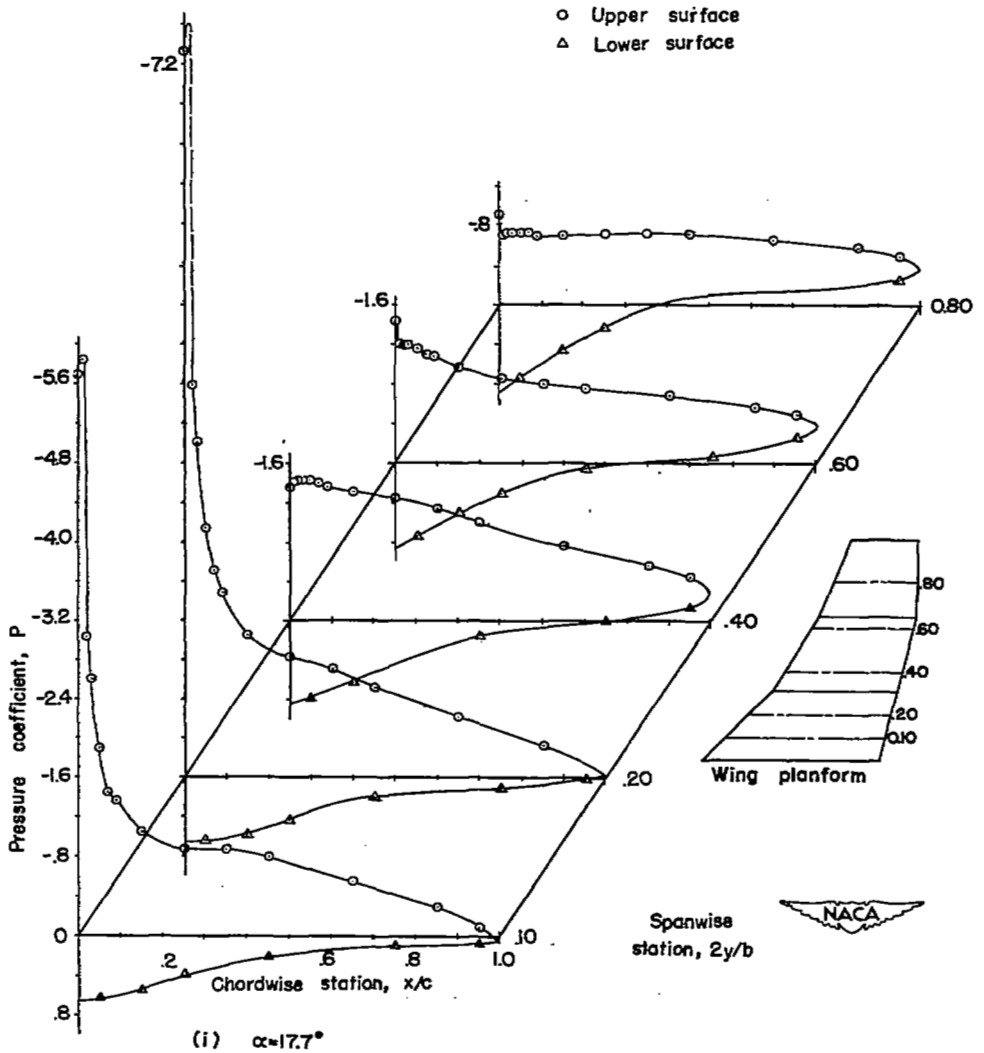

Figure 4.- Continued.

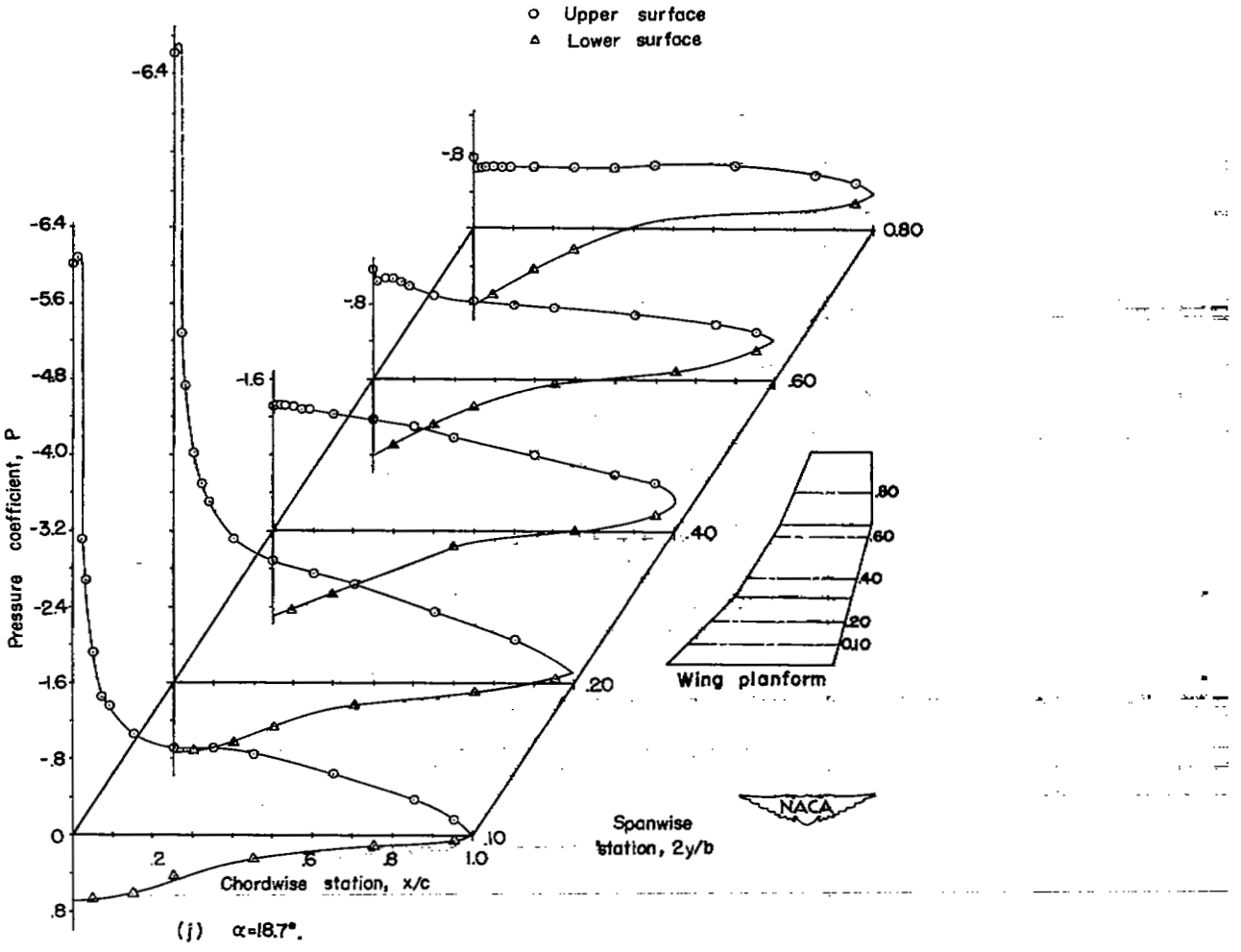

Figure 4.- Concluded.

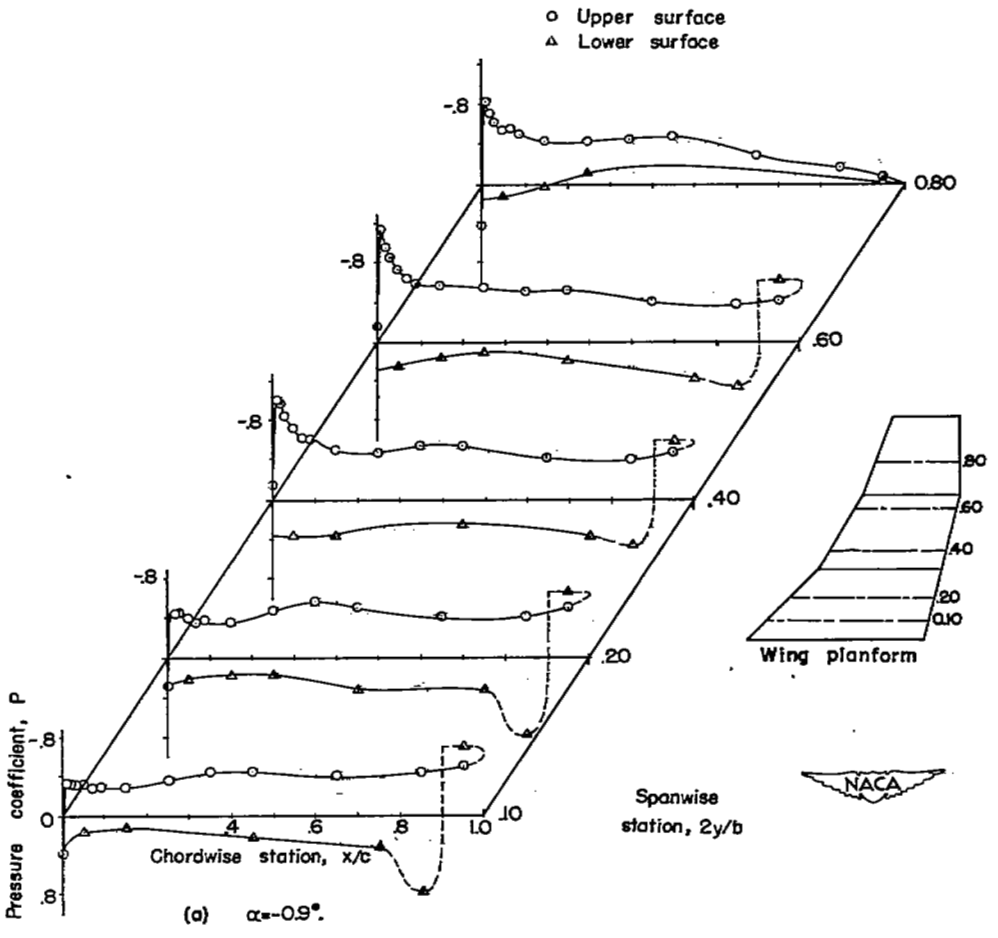

Figure 5.- Pressure distribution along the chord for five spanwise stations at various angles of attack. $\delta_f = -60°$.

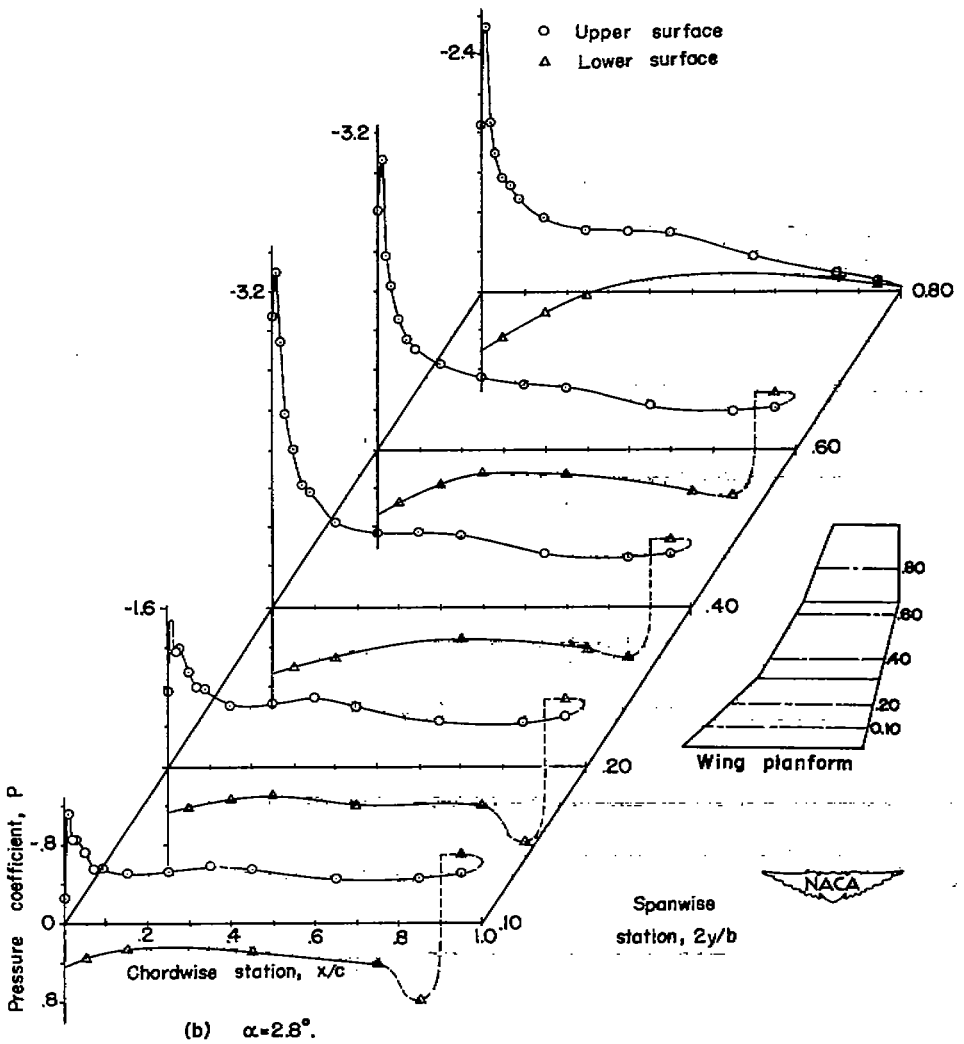

Figure 5.- Continued.

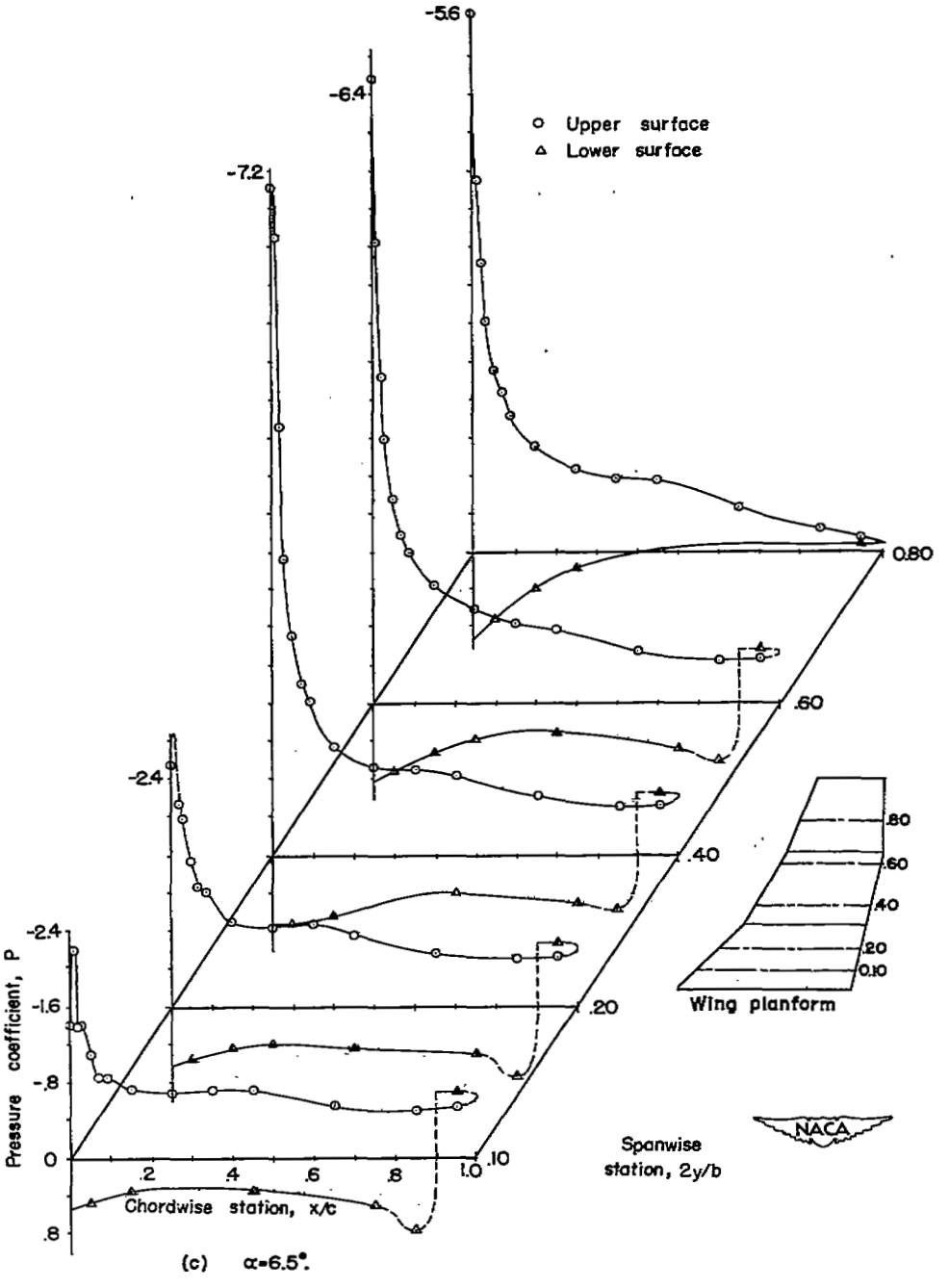

(c) α=6.5°.

Figure 5.- Continued.

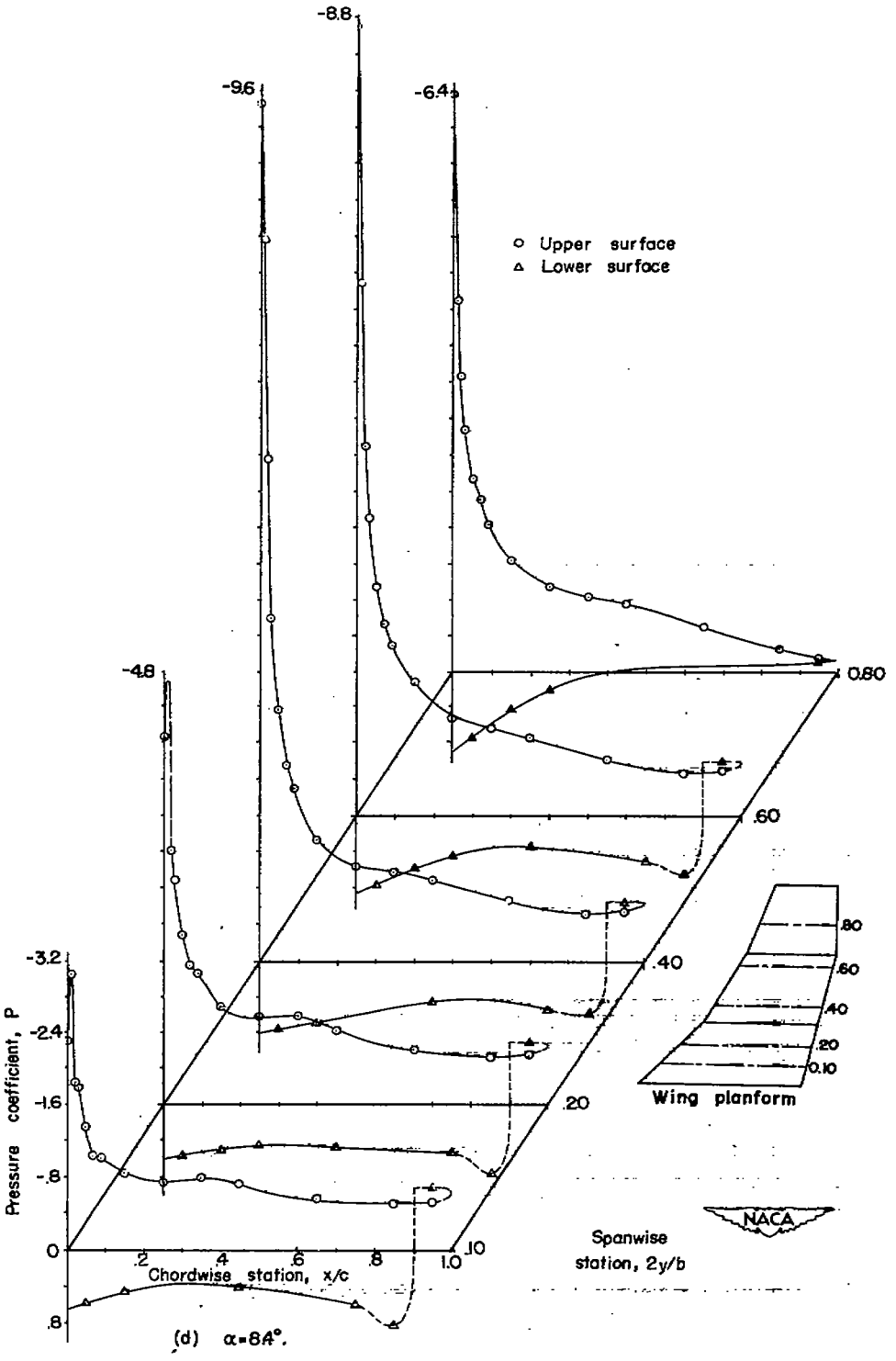

Figure 5.- Continued.

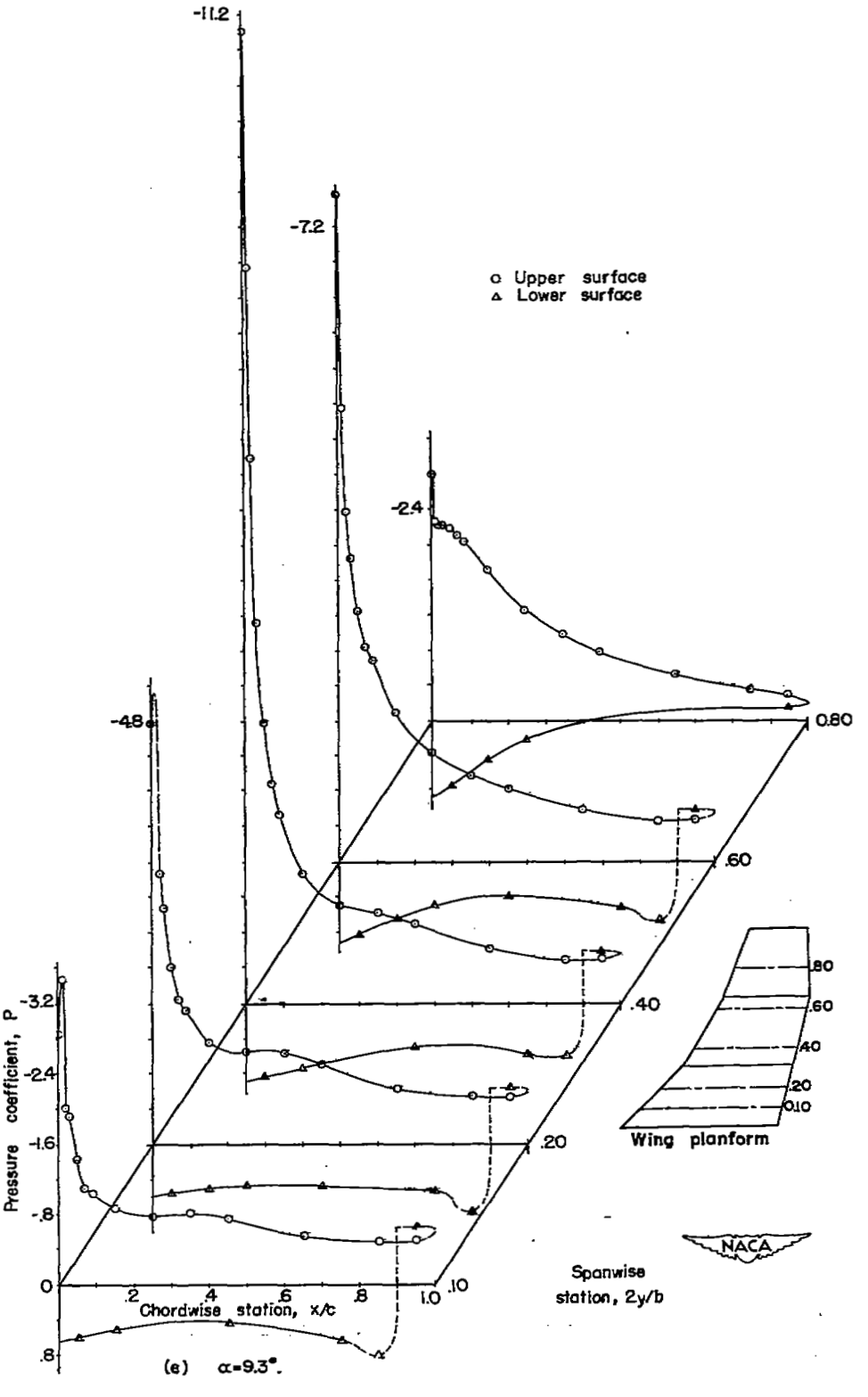

Figure 5.- Continued.

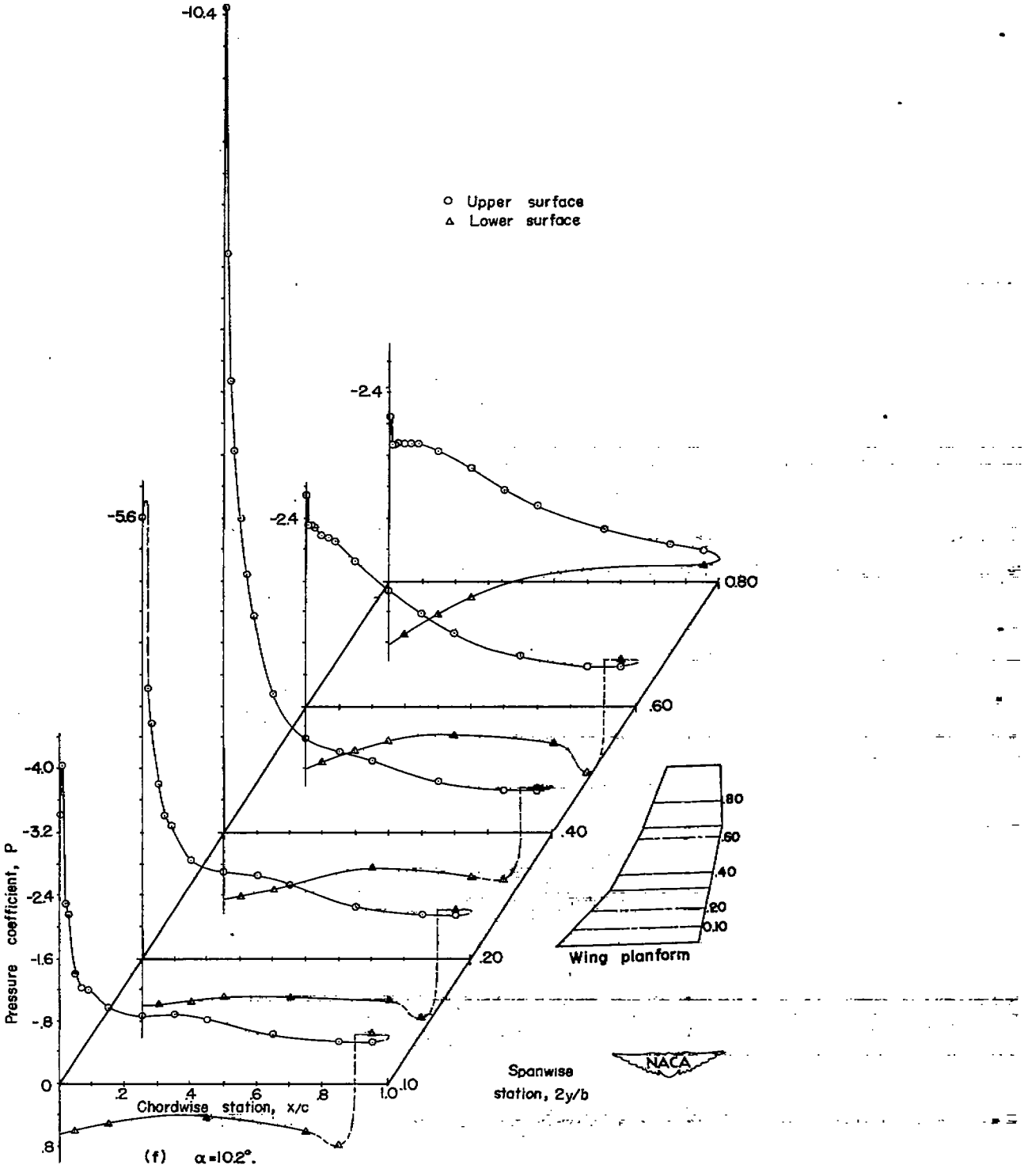

Figure 5.- Continued.

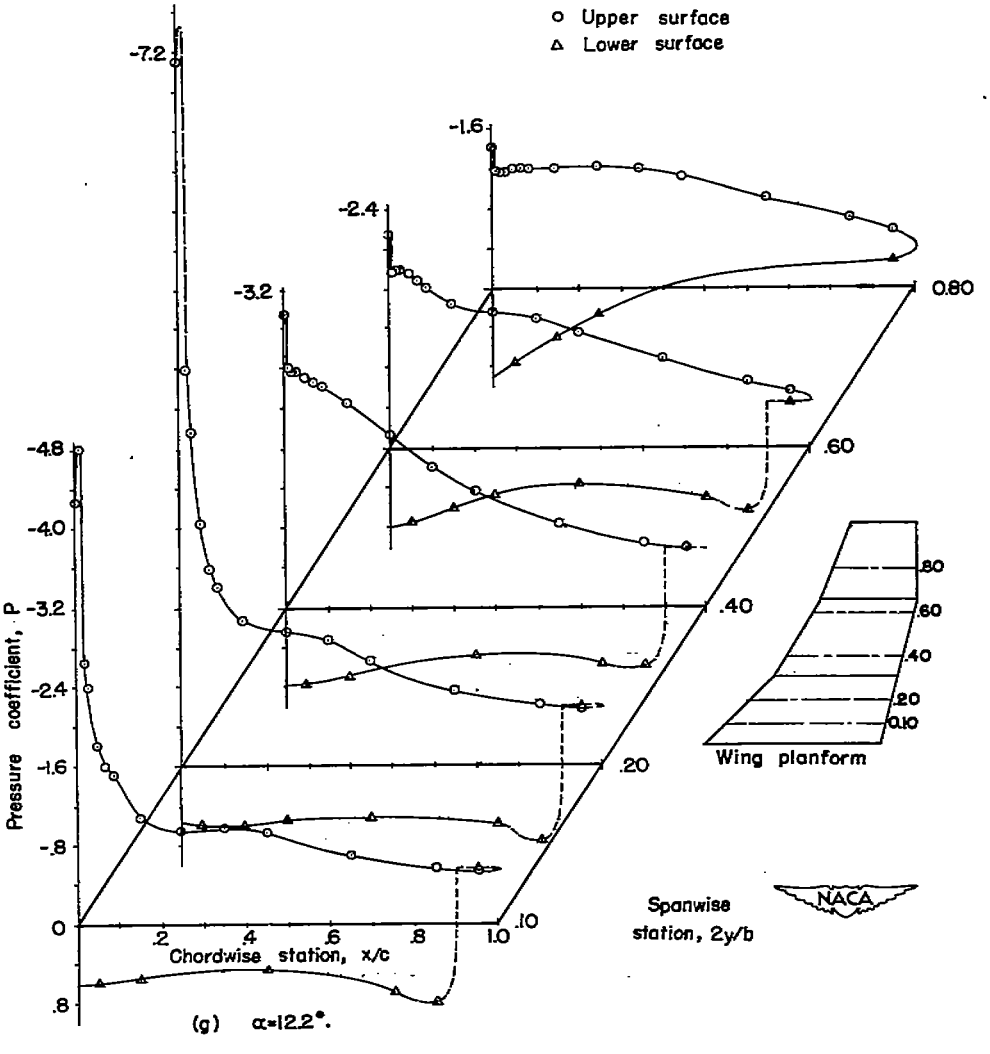

Figure 5.- Continued.

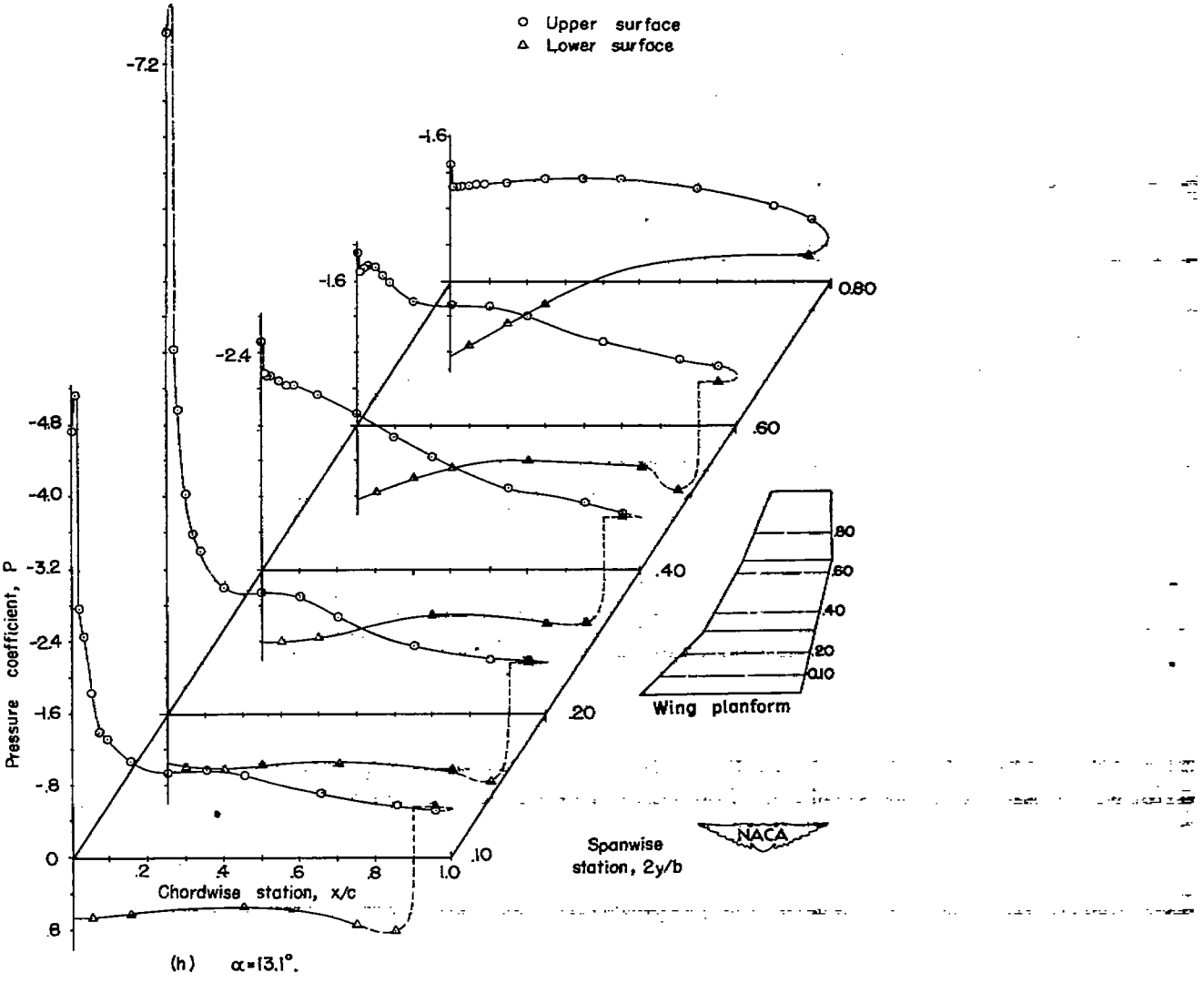

Figure 5.- Concluded.

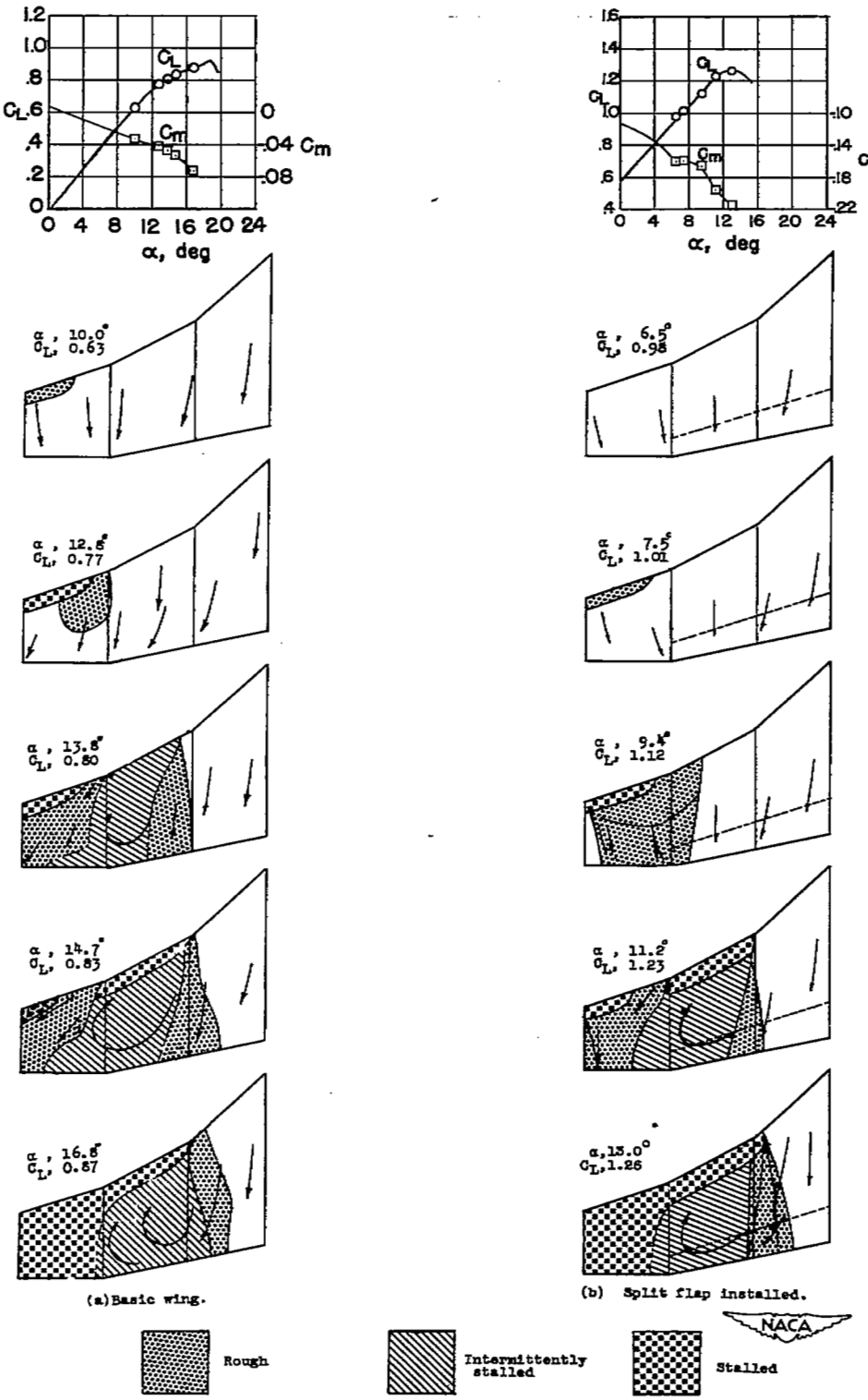

Figure 6.- Flow diagrams. Arrows indicate direction of flow. $R = 3.5 \times 10^6$.

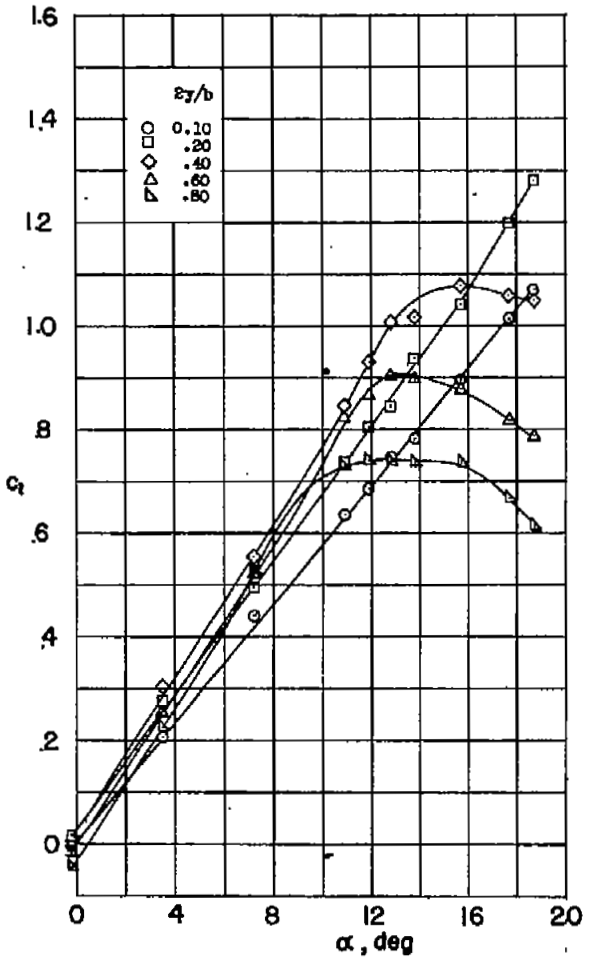

(a) Basic wing.

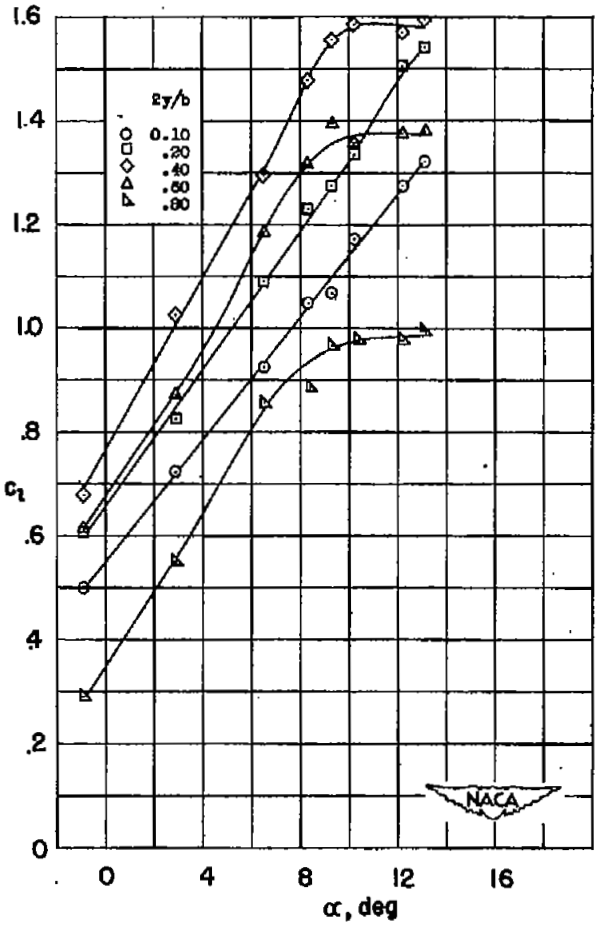

(b) Split flaps installed.

Figure 7.- Variation of section lift coefficient with angle of attack for five spanwise stations.

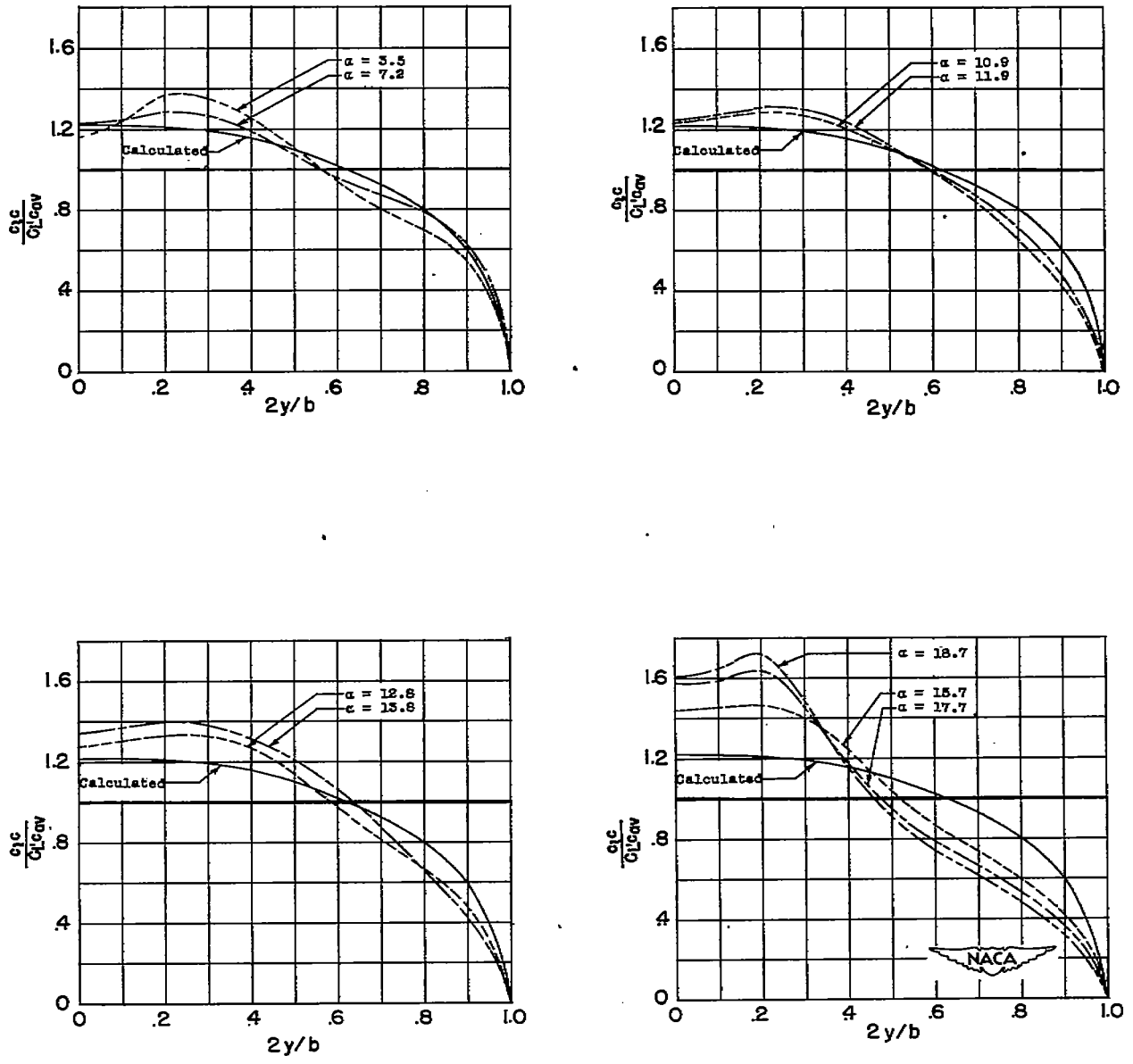

Figure 8.- Spanwise load distribution for various angles of attack. Basic wing.

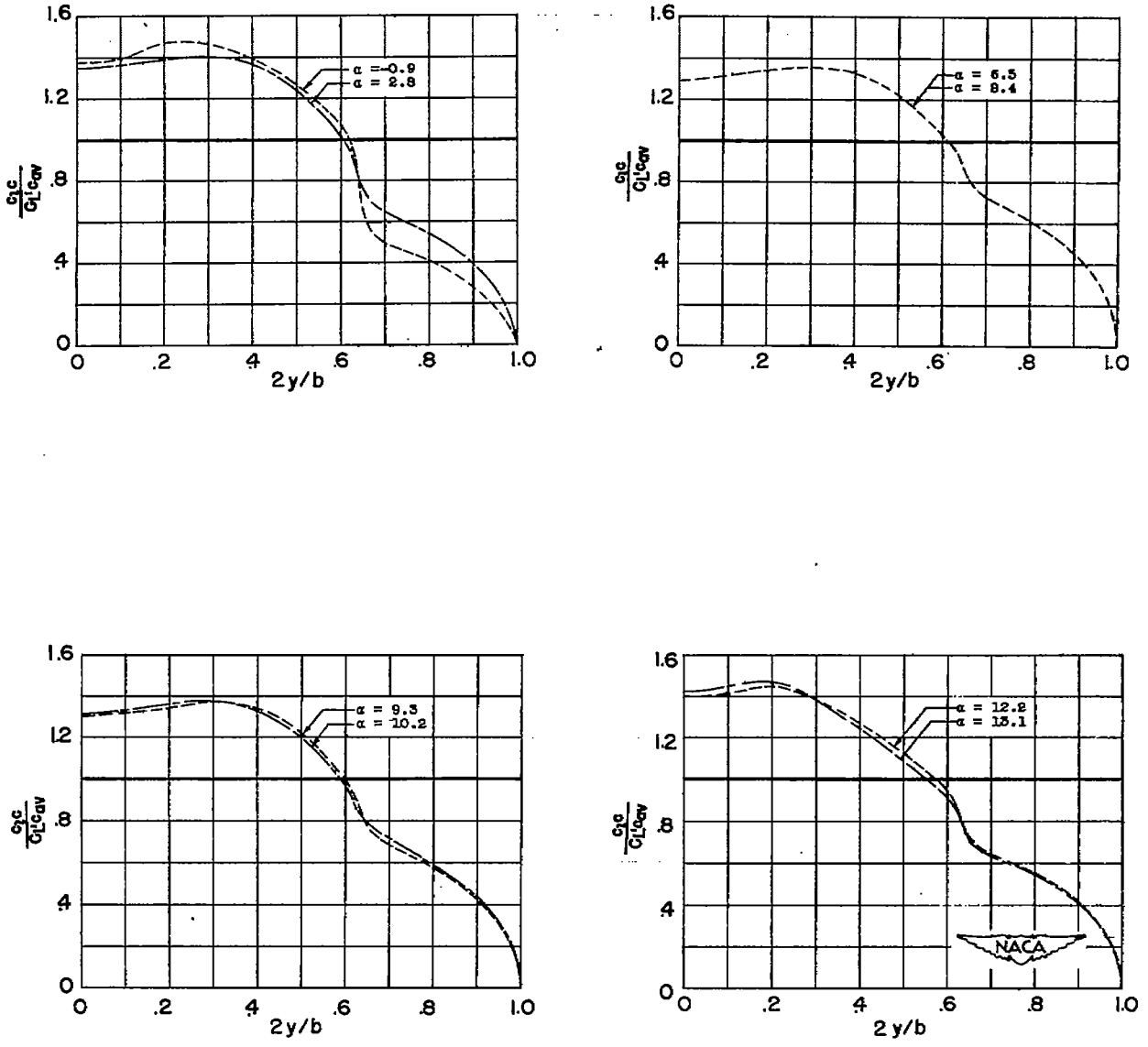

Figure 9.- Spanwise load distribution for various angles of attack. $\delta_f = 60^\circ$.

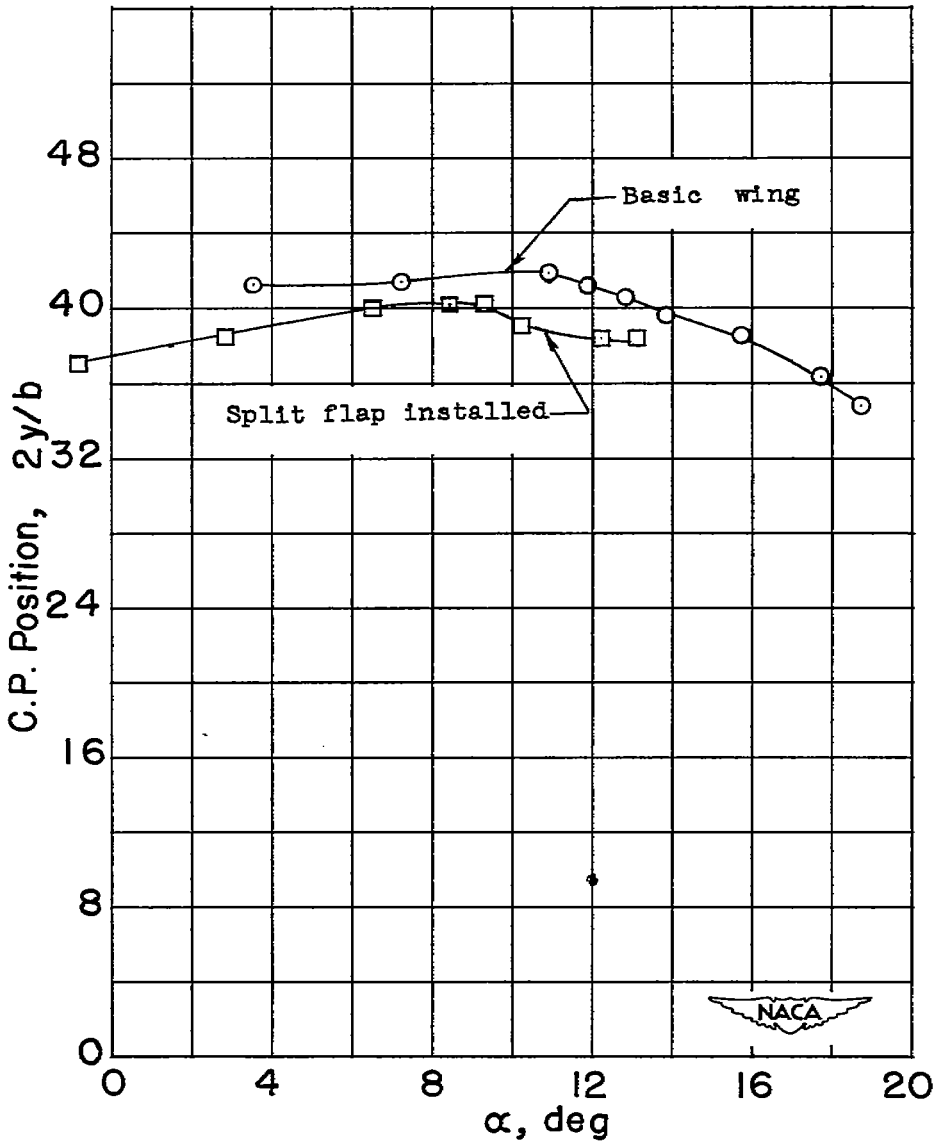

Figure 10.- Variation of spanwise center-of-pressure location with angle of attack.

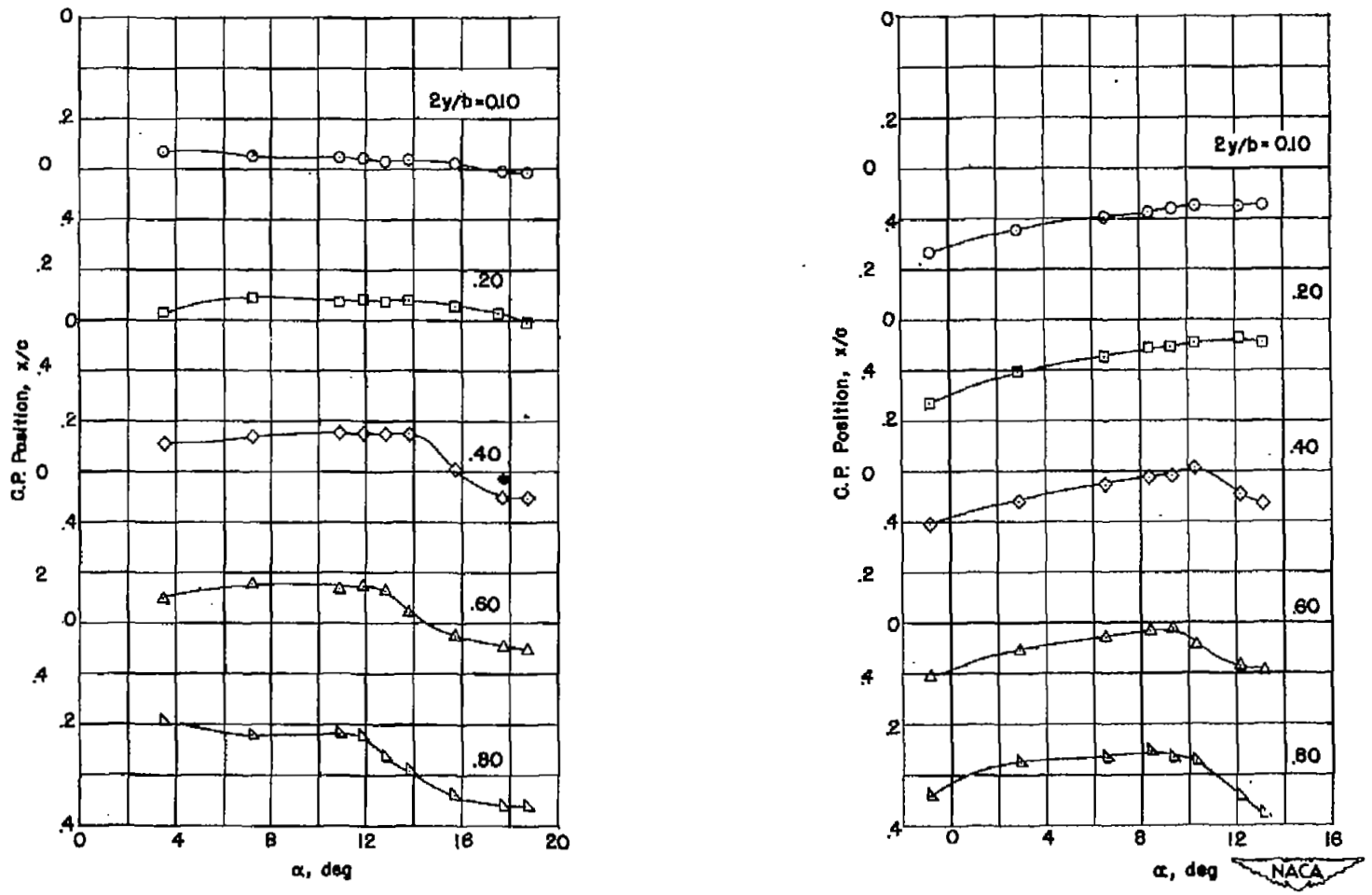

(a) Basic wing.

(b) Split flap installed.

Figure 11.- Variation of center-of-pressure location with angle of attack for five spanwise stations.

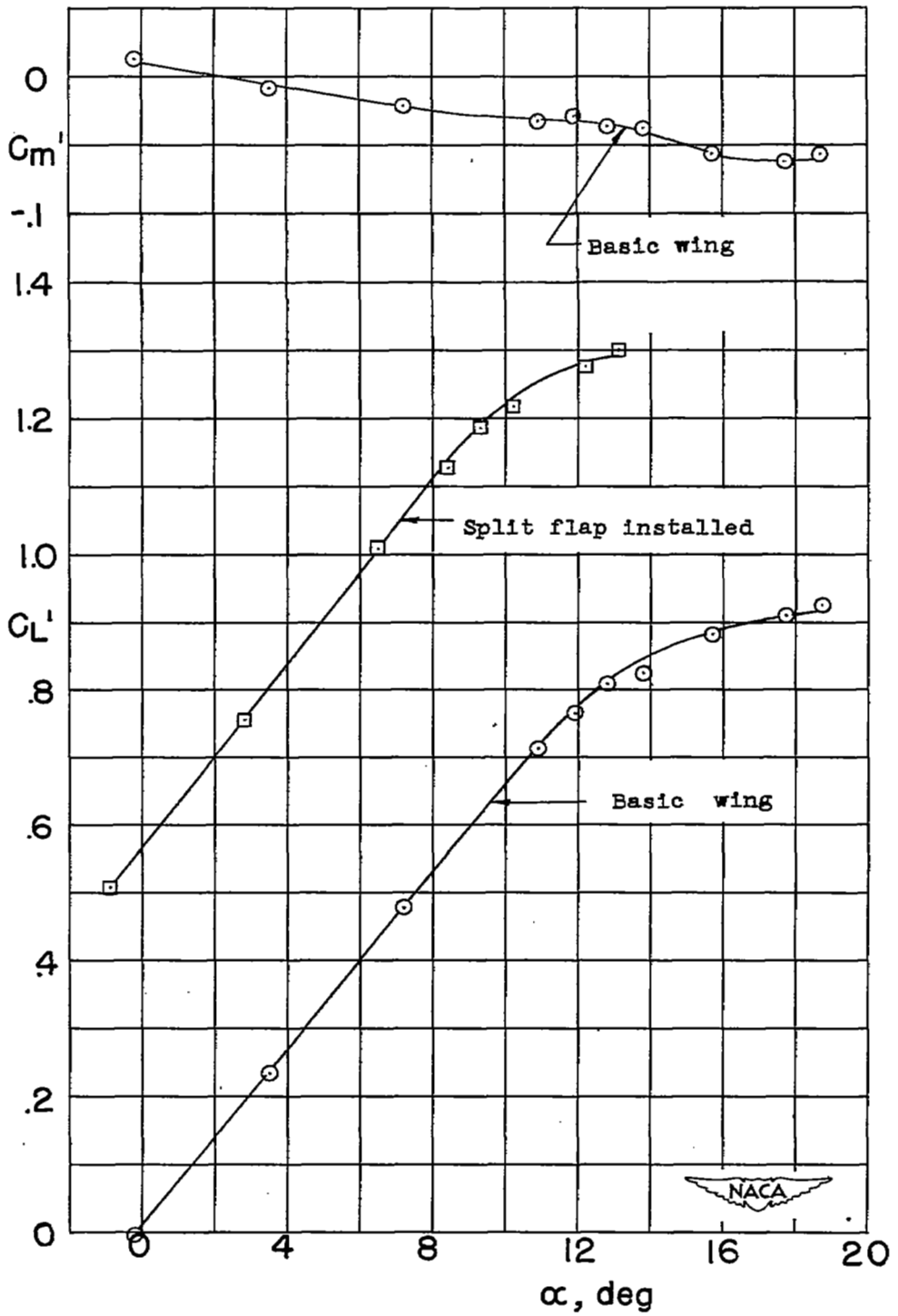

Figure 12.- Variation of total wing lift and pitching-moment coefficients with angle of attack.